KUNS 1341
May 8, 1995

RGM Study of the Hyperon-Nucleon Interaction in the SU_6 Quark Model II.

— Analysis of ΛN - $\Sigma N(I = 1/2)$ Coupled-Channel System —

Yoshikazu Fujiwara

Department of Physics, Kyoto University, Kyoto 606-01

Choki Nakamoto

Graduate School of Science and Technology, Niigata University, Niigata 950-21

Yasuyuki Suzuki

Department of Physics, Niigata University, Niigata 950-21

Abstract

A detailed quark-model study of the ΛN - $\Sigma N(I = 1/2)$ system is given in a coupled-channel formulation of the RGM-F which is recently introduced to achieve a unified understanding of the NN and hyperon-nucleon interaction. It is found that the effect of the ΛN - ΣN transition potential is strongly enhanced in the threshold region through important roles of the non-central components. The antisymmetric $LS^{(-)}$ force, which is characteristically strong in the quark model with the full Fermi-Breit interaction, reproduces a prominent bump structure in the ΛN total scattering cross sections at the energy slightly below the ΣN threshold.

§1. INTRODUCTION

In spite of the basic importance in the study of hypernuclei, our present understanding of the hyperon-nucleon (YN) interaction is quite unsatisfactory in the sense that many different versions of the one-boson exchange potentials (OBEP) are not discriminated due to the scarce experimental information.[1] Since hyperons and nucleons belong to the same class of the spin-flavor SU_6 supermultiplet 56, the rich flavor symmetry of the quark model will provide a strong constraint in which the YN interactions for various hyperons are consistently described with the well-known NN interaction.

We have recently developed a unified description of the NN and YN interactions in the $(3q)$-$(3q)$ resonating-group method (RGM) with a minimum augmentation of effective meson-exchange potentials.[2),3)] This model, which we call RGM-F,† incorporates the full Fermi-Breit interaction with explicit flavor symmetry breaking (FSB) due to the mass difference of the up-down and strange quarks. Besides the well-known short-range repulsion originating from the color-magnetic interaction and the Pauli principle, the spin-dependent central, LS, and the short-range tensor forces are nicely described in this model. (See Ref. 5) for the LS and $LS^{(-)}$ forces.) However, since the important medium-range attraction and the long-range tensor force are never described by any kinds of the quark model, the RGM-F introduces between quarks the central force of the scalar-meson-nonet exchange potentials and the π, K tensor force of the Nijmegen model-F[6)]. The space-spin parts of the exchange kernels for these effective meson-exchange potentials are explicitly calculated by assuming the SU_3 relations of the coupling constants at the baryon level.[3)] Owing to the appropriate reduction of attractive components from NN to ΛN and ΣN in the original Nijmegen model-F parameters, we only need to introduce a common adjustable parameter c for each of the flavor symmetry; $c = 0.4212$ for $\mathcal{P} = a$ (^3E or ^1O) and $c = 0.56$ for $\mathcal{P} = s$ (^1E or ^3O) for the central meson-exchange potentials. These values are determined from the fit to

† A preliminary result of this investigation is given in Ref. 4).

the deuteron binding energy and to the $^1S_0$ phase shift of the NN system, respectively. No adjustment is made for the tensor force of the pseudo-scalar mesons. The mass ratio of the strange to up-down quarks is assumed to be $\lambda = m_s/m_{ud} = 1.25$. The Coulomb force is also introduced in pp and Σ^+p systems in a similar way to the meson exchange potentials.

In this paper, we extend the previous study[3] of RGM-F for the NN and Σ^+p systems to the coupled-channel system with the hypercharge $Y = 1$ and the isospin $I = 1/2$, ΛN - $\Sigma N(I = 1/2)$, in which the approximate SU_3-invariant Hamiltonian mixes these configurations not only through the central component but also through the very rich spin-flavor contents of the non-central forces shared by the YN interaction. It will be found that the RGM-F reproduces all the low-energy cross-section data of the YN scattering up to $p_{lab} = 200$ MeV/c, as well as the gross features of the NN phase shifts. In this energy region, the cross sections are mainly determined by the low-energy behavior of the S-wave phase shifts. At higer energies where the P-wave becomes important, one will find that the antisymmetric $LS^{(-)}$ force plays an important role in the strong coupling of the ^3P and ^1P channels of these $I = 1/2$ configurations, yielding a prominant bump structure at the energy region slightly below the ΣN threshold.

In the next section, the coupled-channel RGM formulation of RGM-F given in Ref. 3) is further elaborated for the ΛN - $\Sigma N(I = 1/2)$ system with a particular emphasis on the detailed treatment of the reduced-mass term and of the effective meson-exchange potentials. The simple prescription in Refs. 2) and 3) enables us to transform the calculated reduced mass to the empirical reduced mass, and to replace the flavor-singlet coupling constants with the phenomenological coupling constants at the baryon level. This needs further refinement when it is applied to the coupled-channel RGM equation with different types of YN configurations. This is particularly important in the $^1S_0$ state of the ΛN - $\Sigma N(I = 1/2)$ system, where a complete Pauli-forbidden state exists. The phase-shift behavior of the ΛN and $\Sigma N(I = 1/2)$ channels and their coupling features in the reflection and transmission coefficients are discussed in § 3.1. The effective-range parameters of the ΛN scattering are also discussed in this subsection. The total and differential cross sections of the Λp and $\Sigma^- p$

systems are discussed in § 3.2. under the approximation with the Coulomb force omitted. The final section is devoted to a summary and an outlook for the further improvement of this investigation.

§2. COUPLED-CHANNEL RGM FORMULATION FOR ΛN - $\Sigma N(I = 1/2)$ SYSTEM

When applying the coupled-channel RGM formulation given in Eq. (2.2) of Ref. 3) to the ΛN - $\Sigma N(I = 1/2)$ system, we need some careful consideration on the reduced-mass term and on the coupling constants of the effective meson-exchange potentials. First of all, the prescription we have introduced in § 4 of Ref. 2) to transform the calculated reduced mass to the empirical one cannot straightforwardly be applied in the present case, since the empirical reduced mass μ_1^{exp} for ΛN system and μ_2^{exp} for ΣN system are different. (From now on, the channel indices $\alpha = 1$ and $\alpha = 2$ are used to stand for ΛN and ΣN channels, respectively, by assuming that the first channel is always the incident channel. For the ΣN incident channel, 1 and 2 are reversed.) One may imagine that an extension of Eq. (4.2) in Ref. 2) to the channel-coupling case can easily be done by replacing the off-diagonal exchange kernels $\mathcal{M}^{(K)}_{\alpha\alpha'}(\boldsymbol{R}, \boldsymbol{R}')$ and $\mathcal{M}^{(MC)}_{\alpha\alpha'}(\boldsymbol{R}, \boldsymbol{R}')$ with

$$\widetilde{\mathcal{M}}^{(\Omega)}_{\alpha\alpha'}(\boldsymbol{R}, \boldsymbol{R}') = \sqrt{\frac{\mu_\alpha \mu_{\alpha'}}{\mu_\alpha^{exp} \mu_{\alpha'}^{exp}}}\, \mathcal{M}^{(\Omega)}_{\alpha\alpha'}(\boldsymbol{R}, \boldsymbol{R}') \qquad \text{for} \quad \Omega = K \quad \text{and} \quad MC \ , \tag{2.1}$$

but this procedure leads to the unfavorable fact that the Pauli principle is not always satisfied. To illustate this, we consider the most compact $(0s)^6$ harmonic oscillator (h.o.) configuration, which is a complete Pauli-forbidden state in the spin-flavor SU_6 coupling $1/2(11) \times 1/2\,(11) \to 0\,(11)_s$. The explicit values of the spin-flavor-color factors X_N of the exchange normalization kernel are given by

$$X_N = \begin{pmatrix} 0 & -\frac{1}{3} \\ -\frac{1}{3} & -\frac{8}{9} \end{pmatrix} \tag{2.2}$$

in 2×2 matrix form of the ΛN and ΣN channel coupling. One of the eigen-vectors of Eq. (2.2), $\begin{pmatrix} 1 \\ 3 \end{pmatrix}$, satisfies

$$\left[\begin{pmatrix} 1 & 0 \\ 0 & 1 \end{pmatrix} + \begin{pmatrix} 0 & -\frac{1}{3} \\ -\frac{1}{3} & -\frac{8}{9} \end{pmatrix}\right]\begin{pmatrix} 1 \\ 3 \end{pmatrix} = 0 \ . \tag{2.3}$$

As is well known in the nuclear cluster problems, an important result of this fact is that a set of $(0s)$ h.o. wave functions $\{\chi_\alpha^{FBS}(\boldsymbol{R})\}=(1/\sqrt{10})\ (\chi_{(0s)}^{h.o.}(\boldsymbol{R}),\ 3\,\chi_{(0s)}^{h.o.}(\boldsymbol{R}))$ forms a redundant state (the Pauli-forbidden state) which trivially satisfies the coupled-channel RGM equation Eq. (2.2) of Ref. 3). This is usually called the redundancy condition. If the exchange kernels of the kinetic-energy type are modified to Eq. (2.1) and the empirical reduced masses are employed in the kinetic-energy term and the relative-energy expression, the redundancy condition is no longer satisfied. Similarly, it is not satisfied either for the effective meson-exchange potentials unless the direct potentials and the corresponding exchange kernels are exactly calculated, starting from the qq interaction assumed in the original Hamiltonian. Since we have evaluated the coupling constants of the meson-exchange potentials in such a way that the direct potentials are reduced to the OBEP of the Nijmegen model-F, the present approximation of the RGM-F clearly breaks the redundancy condition.

In the present application to the ΛN-$\Sigma N(I=1/2)$ system, these approximate treatments of the Pauli principle in fact impairs the scattering solutions very little, since the effect of the Pauli principle is usually very weak except for the $^1S_0$ state discussed above. For example, another compact S-wave configuration for the ^3S state with $(0s)^6$ and $S(\lambda\mu)_\rho = 1(11)_a$ quantum numbers has the norm eigen-value $1+X_N = 8/9$, indicating that the effect of the quark antisymmetrization is very weak. On the other hand, the $^1S_0$ phase-shift behavior is strongly affected by the redundant component admixed due to the present approximation. We cure this flaw of RGM-F by slightly modifying the spin-flavor-color factors in the non-incident channel in the following way. Let us consider only the spin-flavor-color parts since the spatial part is totally symmetric for the $(0s)^6$ configuration. We modify the relationship Eq. (2.3) in such a way that the redundancy condition is still satisfied even when the direct term takes the form of any arbitrary 2×2 symmetric matrix with three independent elements a, b and c;

$$\left[\begin{pmatrix} a & b \\ b & c \end{pmatrix} + \begin{pmatrix} 0 & -\frac{1}{3}B \\ -\frac{1}{3}B & -\frac{8}{9}C \end{pmatrix}\right]\begin{pmatrix} 1 \\ 3 \end{pmatrix} = 0 \ . \tag{2.4}$$

The modification factors B and C of the exchange kernel are determined from a, b and c as

$$B = a+3b \ , \qquad C = \frac{1}{8}(9c-a) = c+\frac{1}{8}(c-a) \ . \tag{2.5}$$

When applying this to the kinetic-energy term, we choose $a=\mu_1/\mu_1^{exp}$, $b=0$ and $c=\mu_2/\mu_2^{exp}$, resulting in $B=a$ and $C=c+(1/8)(c-a)$. This modification is slightly different from that of Eq. (2.1). This procedure, however, does not work when the scattering problem with ΣN incident channel is considered. This is because the X_N value for the ΛN diagonal channel happens to be exactly zero. In this particular case, we assume a small but non-zero value X_2 for this factor and consider the condition

$$\left[\begin{pmatrix} a & b \\ b & c \end{pmatrix} + \begin{pmatrix} -\frac{8}{9}A & -\frac{1}{3}B \\ -\frac{1}{3}B & X_2C \end{pmatrix}\right]\begin{pmatrix} 3 \\ 1 \end{pmatrix} = 0 \ . \tag{2.6}$$

By supplementing an extra condition $A=a$, we find from Eq. (2.6)

$$B = a+3b \ , \qquad X_2C = a-c \ . \tag{2.7}$$

Namely, we can set $C=c$ and $X_2 = a/c-1$ which would be zero if $a=c$. The condition $A=a$ is required to guarantee that the present approximation reduces to the previous one in the single-channel case.

It should be noted that the redundancy condition should be satisfied even when the FSB is introduced. From the careful analysis of the generator-coordinate (GCM) kernels, we find that a rather involved term which is not proportional to the factor X_N in the exchange kernels of the kinetic-energy and momentum-dependent retardation terms does not contribute to the $(0s)^6$ configuration. Therefore, the above discussion directly applies to these exchange kernels when the ΛN channel is selected as the incident channel. On the other hand, if the ΣN channel is adopted as the incident channel, we actually modify the spin-flavor-color factors in the ΛN channel as $X_N = 0 \rightarrow X_N = \rho_1 - \rho_2$ in $\mathcal{M}_{22}^{(K)}(\boldsymbol{R},\boldsymbol{R}')$

and $X_E^{MC} \to X_E^{MC} - (2+1/\lambda)(\rho_1 - \rho_2)$ in $\mathcal{M}_{22}^{(MC)}(\boldsymbol{R}, \boldsymbol{R}')$, where $\rho_i = \mu_i/\mu_i^{exp}$ $(i = 1, 2)$ and X_E^{MC} is the E-type spin-flavor-color factor of the MC-type exchange kernel. For the effective meson-exchange potentials, the present approximation described in § 2 of Ref. 3) is equivalent to multiplying each component of the exchange kernels by the corresponding direct factor a, b or c. Since the spin-flavor-color factors of the scalar-meson central force are proportional to X_N, we can also apply the above prescription to the RGM kernels in the $^1S_0$ state. The tensor-type factors are not affected for this spin-singlet state. We should also note that the reciprocity theorem is not exactly satisfied for the $^1S_0$ state in the present prescription.

Next, let us briefly discuss the treatment of the threshold energies in RGM-F. In the single-channel RGM formulation, the internal energies of clusters do not show up in the RGM equation, since they are already subtracted from the exchange kernel. This is not the case for the multi-configuration RGM equation, where the difference of the internal energies of different channels should be explicitly evaluated from the original Hamiltonian. In the present ΛN-$\Sigma N (I = 1/2)$ system, the mass difference

$$\Delta E = E_\Sigma - E_\Lambda = \sqrt{\frac{2}{\pi}} \alpha_S \left(\frac{1}{m_{ud} b}\right)^3 m_{ud} \left(1 - \frac{1}{\lambda}\right) \frac{4}{9} \tag{2.8}$$

from the color-magnetic interaction is the only source of the Λ-Σ mass splitting, since the present approximation of the effective meson-exchange potential does not yield any contributions. Since we use $\lambda = 1.25$ in the present calculation, we obtain the mass difference $\Delta E = 39.11$ MeV, about a half of the empirical threshold energy $\Delta E = 77.49$ MeV. In a more advanced version of RGM-F, we will show that this discrepancy is reduced by a more proper treatment of the flavor dependence of the meson-exchange potentials. In what follows, we have to note that the "theoretical" ΣN channel opens at the momentum $p_\Lambda = p_{beam} = 445.2$ MeV/c, though the corresponding empirical momentum is actually $p_{beam}^{exp} = 637.9$ MeV/c. In these estimations, we have employed the relationship between the non-relativistic relative energy E_{rel}^{NR} in the center of mass system and the beam momentum p_{beam} given through [9]

$$\begin{aligned}
E_{beam} &= \sqrt{m^2 + p_{beam}^2} = m + T_{beam} \ , \\
E_{cm} &= \sqrt{m^2 + M^2 + 2M E_{beam}} = \sqrt{(m+M)^2 + 2M T_{beam}} \ , \\
p_{cm} &= p_{beam} \frac{M}{E_{cm}} \ , \\
E_{rel}^{NR} &= \frac{p_{cm}^2}{2\mu} = \frac{M}{m+M} \frac{T_{beam}\left(1 + \frac{1}{2m} T_{beam}\right)}{1 + \frac{2M}{(m+M)^2} T_{beam}} \ ,
\end{aligned} \tag{2.9}$$

where $\mu = mM/(m+M)$ is the non-relativistic reduced mass with m and M being the masses of the incident and target particles, respectively.

The coupled-channel RGM equations for the ΛN-$\Sigma N (I = 1/2)$ system are solved by a variational technique developed by Kamimura [7]. From the resultant relative-motion functions, we extract the scattering matrix $S_{\alpha\alpha'}$, which is customarily parametrized as

$$S_{\alpha\alpha'} = \eta_{\alpha\alpha'} e^{2i\delta_{\alpha\alpha'}} \ , \tag{2.10}$$

where $\eta_{\alpha\alpha'} = |S_{\alpha\alpha'}|$ are the reflection and transmission coefficients for $\alpha = \alpha'$ and $\alpha \neq \alpha'$, respectively. These coefficients and the diagonal phase shifts $\delta_{\alpha\alpha}$ are discussed in § 3.1. The number of channels specified by $^{2S+1}L_J$ with the total spin S and the partial wave L is at most four for each total angular momentum J with some definite parity, if one neglects the isospin breaking. The coupling of the ^1L_J and ^3L_J partial waves by the antisymmetric $LS^{(-)}$ force is also explicitly incorporated.

§3. RESULTS AND DISCUSSION

3.1. Analysis of the Phase Shifts

The $^1S_0$ phase-shift curves of the ΛN and $\Sigma N (I = 1/2)$ channels are shown in Fig. 1, together with the Λp phase shift predicted by the Nijmegen model-F [6] (crosses). These two curves are obtained by choosing the ΛN channel as the primary channel. We find that the present calculation yields very reasonable result of the ΛN phase shift comparable to the model-F prediction especially in $p_\Lambda < 400$ MeV/c region. In Fig. 1, the ΛN single-channel

phase shift is also shown by the dashed curve. One finds that the channel-coupling effect in this case is rather moderate, except for the cusp region in which the appearance of the Wigner cusp is a common feature of the S-wave phase shifts without the Coulomb force. In the low-energy region where the ΣN channel is closed, the phase-shift difference between the single-channel and coupled-channel calculations is at most $7 \sim 8°$. The weak-coupling feature at higher energies above the threshold is also observed in the transmission coefficients between the two channels (not shown). They are found to be less than 0.6 in all the energy region below $p_\Lambda = 1$ GeV/c.

An interesting enhancement of the ΛN - ΣN coupling is found in $^3S_1$ phase shift shown in Fig. 2, when the tensor force from the π- and K-meson exchange potentials is incorporated. In this case, the RGM equation is composed of the following four channels; ΛN $^3S_1$, ΛN $^3D_1$, $\Sigma N(I = 1/2)$ $^3S_1$ and $\Sigma N(I = 1/2)$ $^3D_1$, which we call 1, 2, 3 and 4, respectively. Let us first discuss the scattering from the ΛN channel. The ΛN phase shift in Fig. 2 shows the effect of the channel-coupling is appreciable, reaching $12 \sim 13°$ difference from the ΛN single-channel result. Owing to this appreciable effect, the resultant phase-shift values show very nice correspondence to the model-F result in the almost full energy region. The threshold effect found as the cusp structure in the $^1S_0$ state now appears as a sharp step-like resonance at the calculated ΣN threshold with $p_\Lambda = 445.2$ MeV/c. Figure 3 shows the ΛN $^3D_1$ phase shift and the mixing parameter ϵ_1 for $^3S_1$ - $^3D_1$ coupling. In this paper, we follow the standard definition of the nuclear bar phase shifts for the mixing parameter in the two-channel S-matrix. In Fig. 3, the predictions of the Nijmegen model-D [8] are also shown with open circles. Except for the difference of the threshold energies between RGM-F and the Nijmegen models, the behavior of the ΛN $^3D_1$ phase shift and ϵ_1 is rather similar between these two models. It is interesting to note that the model-D and model-F predict different signs for ϵ_1, and the result of RGM-F is rather close to that of model-D.

The behavior of the reflection and transmission coefficients at the threshold region is plotted in Fig. 4(a) for the scattering with ΛN incident channel and in Fig. 4(b) for that with ΣN channel. From the curve for η_{21} in Fig. 4(a), we find that the $^3S_1$ and $^3D_1$ channels

of the ΛN configuration strongly couple to each other only in the very narrow region of the thereshold energy. Apparently this is initiated by the combined effect of the ΛN - ΣN coupling and the tensor force, since the dashed curves in Figs. 2 and 3 show smooth behavior entirely different from the solid curves. The rather moderate strength of the ΛN - ΣN coupling except for this narrow threshold region is reasonable, since the tensor force in the ΛN system is dominantly contributed from the K-meson exchange through the exchange Feynman diagram.

On the other hand, the ΣN system has the contribution from the π-exchange tensor force in the direct diagram and shows a strong effect of the $^3S_1$-$^3D_1$ coupling. This feature is indeed seen in Fig. 5, where the ΣN phase-shift curves are depicted in various approximations. In Fig. 5, the dotted curve shows the $\Sigma N(I = 1/2)$ single-channel calculation with the tensor force turned off. When all the non-central forces are turned on, we obtain the dashed curve which is the result of the full ΣN single-channel calculation. The maximum value of the phase shift has increased from 20° to 48° mainly due to the tensor force in this ΣN channel. If we further introduce the channel-coupling to the ΛN configuration, we find the very strong attractive nature of the phase shift at low energies. Namely, the ΣN phase shift sharply decreases from 180° to about 90° at $p_\Sigma = 60$ MeV/c.

One may think that this strong coupling of the narrow width between ΛN $^3S_1$ and $\Sigma N(I = 1/2)$ $^3S_1$ channels is caused by the strong one-pion tensor force existing between ΛN $^3S_1$ and $\Sigma N(I = 1/2)$ $^3D_1$ channels, in addition to the above mentioned tensor force in the ΣN channel. However, this does not seem to be the case, since the transmission coefficient η_{41} in Fig. 4(a) does not show a prominent rise. On the other hand, the η_{23} curve in Fig. 4(b) for the $\Sigma N(I = 1/2)$ $^3S_1$ to ΛN $^3D_1$ channels shows a rather sharp rise up to $\eta_{23} = 0.6$. To make sure that this component is actually very important, we show in Fig. 6 the reflection coefficients η_{33} and the transmission coefficients when the channel coupling to ΛN configurations is turned on (solid curves) and off (dashed curves) in the $\Sigma N(I = 1/2)$ scattering. We here find that the above coupling is essential for the sharp resonance behavior at the ΣN threshold.

In Fig. 5, the $\Sigma N(I = 1/2)\ ^1S_0$ phase shift is also shown for comparison with the same curve in Fig. 1. Only difference is that the curve in Fig. 1 is obtained by selecting the ΛN channel as the primary channel, while that in Fig. 5 is by selecting the ΣN channel. As is discussed in § 2, these two curves are not exactly equal in the present treatment. However, if we compare the phase-shift values at the same incident momentum, we find that the difference is rather small. For example, the phase-shift value at $p_\Lambda = 1,000$ MeV/c in Fig. 1 is $-76.15°$, while that in Fig. 5 at the corresponding Σ incident momentum $p_\Sigma = 911.2$ MeV/c through Eq. (2.9) is about $-74°$ and the difference is just a couple of degrees.

In order to make sure that the low-energy behavior of the ΛN S-wave phase shifts is consistent with the available Λp cross section data, we list in Table I the comparison of the singlet and triplet S-wave effective-range parameters predicted by RGM-F with those of the other models and some experimental analyses [10),11)]. We see that these parameters for the ΛN system have very nice correspondence to the values determined by many successful OBEP models like the Nijmegen models [8),6)] and the Jülich models [12)]. In particular, the singlet and triplet scattering lengths satisfy the condition $|a_s| \geq |a_t|$, which is required from the spin assignment of ${}^3_\Lambda$H system.[10)]

Figure 7 shows the phase-shift behavior of the four-channel calculation composed of ΛN $^1D_2$-$^3D_2$ and $\Sigma N(I = 1/2)\ ^1D_2$-$^3D_2$ channels. The antisymmetric $LS^{(-)}$ force couples $^1D_2$ and $^3D_2$ channels. The full calculation reproduces the behavior of the Λp phase shifts of the model-F very nicely.

Next, we discuss P-wave phase shifts in the ΛN and $\Sigma N(I = 1/2)$ systems. For $J = 0$ and 2, the results of the two-channel calculations are given by solid curves in Figs. 8 and 9, respectively. Here we also find that the coupling effect between these two channels is not particularly significant in the whole energy region. In both cases, it increases the attractive feature of the single-channel ΛN phase shifts by up to about 10 degrees. The $\Lambda N\ ^3P_0$ phase shift shows a weak Wigner cusp at the ΣN threshold, while the $^3P_2$ phase shift is appreciably more attractive than either of the model-D or model-F predictions.

A similar feature to the threshold resonance in the $^3S_1$ ΛN phase shift is seen in the four-

channel calculation of the P-wave $J = 1$ system. The $^1P_1$ and $^3P_1$ phase shifts of the ΛN and $\Sigma N(I = 1/2)$ systems are shown in Figs. 10 and 11, respectively, together with the model-F predictions for the ΛN phase shifts. Here one finds that, although the ΛN phase shifts are very small in the single-channel calculations (dashed curves), they gain vigorous resonance behavior through the channel-coupling at $p_\Lambda = 380$ MeV/c, which is about 65 MeV/c below the ΣN threshold. It is important to note that the resonance in the $^3P_1$ channel in Fig. 11 shows the step-like behavior, while that in the $^1P_1$ channel in Fig. 10 shows the dispersion-like behavior. This implies that the resonance state has a larger partial width in the $^3P_1$ channel than in the $^1P_1$ channel.[13)] In order to see that the dominant component of this resonance state lies in the $\Sigma N(I = 1/2)\ ^3P_1$ channel, we show in Fig. 12 the reflection coefficient η_{11} and the transmission coefficients η_{21}, η_{31} and η_{41} for the S-matrix with the $\Lambda N\ ^1P_1$ incident channel. Here, the $\Lambda N\ ^1P_1$, $\Lambda N\ ^3P_1$, $\Sigma N(I = 1/2)\ ^1P_1$ and $\Sigma N(I = 1/2)\ ^3P_1$ channels are denoted by 1, 2, 3 and 4, respectively. The coefficient η_{41} has a very sharp rise at the threshold and increases up to $\eta_{41} = 0.7$ at $p_\Lambda = 1$ GeV/c.

The origin of this resonance is in fact the weak attraction already found in the $\Sigma N(I = 1/2)\ ^3P$ central phase shift discussed in Ref. 2). In order to see this, we show in Fig. 13 how the $\Sigma N(I = 1/2)\ ^3P_1$ phase shift changes with the successive introduction of various pieces of interactions. The ^3P phase shift calculated only with the central force (dotted curve) shows weak attraction up to 25° at $p_\Sigma = 800$ MeV/c. It is strongly enhanced by the LS and tensor non-central forces and reaches 60° at the maximum value (dot-dashed curve). The introduction of the $LS^{(-)}$ force further enhances this attractive effect through the coupling with the $^1P_1$ channel of the $\Sigma N(I = 1/2)$ system (dashed curve). The phase shift goes beyond 90° at $p_\Sigma = 260$ MeV/c. Further extension of the model space through the coupling with the ΛN channel suddenly pushes this resonance away to the $^3P_1$ state of the ΛN channel, where the very prominent broad step-like resonance appears as in Fig. 11. This interesting effect of the $LS^{(-)}$ force in the ΛN-ΣN coupled-channel problem is not introduced in the Nijmegen model, which gives very smooth behavior in Figs. 10 and 11.

Quite clearly, this is related to the fairly strong $LS^{(-)}$ force predicted in the quark model

with the full Fermi-Breit interaction[5]. Unlike the $\Sigma N(I=3/2)$ channel, the $\Sigma N(I=1/2)$ and ΛN channels gain a very strong effect of the $LS^{(-)}$ force which causes the transition between the symmetric and antisymmetric octet configurations, $(11) \times (11) \to (11)_s$ and $(11)_a$, even for the SU_3-scalar Hamiltonian with exact flavor symmetry. Since the flavor symmetric $\Sigma N(I=1/2)$ configuration contains the $(11)_s$ component with 90 % (see Table I of Ref. 2)), the effect is apparently the strongest for the transitions to the $\Sigma N(I=1/2)$ channel. Here we again find the phenomenon that the rather insignificant ΛN - $\Sigma N(I=1/2)$ coupling in each of the ${}^3P_1$ and ${}^1P_1$ channels is strongly enhanced by the non-central force, this time, the $LS^{(-)}$ force.

3.2. Total and Differential Cross Sections

The calculated total cross sections for the Λp scattering are compared with the experimental data[10),11),14)] in Fig. 14. A broad bump in the energy region $p_\Lambda = 300 \sim 500$ MeV/c is a consequence of the prominent resonance structure in ${}^3P_1$ and ${}^1P_1$ states discussed in the preceding subsection. The agreement with the experiment is fairly good except for the last two high-momentum data points at $p_\Lambda = 290$ and 300 MeV/c by the Rohovoth-Heidelberg collaboration[10] and by the Maryland group[11]. We should, however, note that the present calculation gives too small threshold energy for the ΣN configuration. In a more realistic calculation with the correct threshold energy, it is probable that the peak position shifts to the higher momentum region and the peak height becomes much lower. Furthermore, the threshold resonance of the ${}^3S_1$ and ${}^3D_1$ states appearing in the Nijmegen models[6),8)] and the quark model in Ref. 15) does not seem to show up clearly in this calculation. This is probably because the width of this resonance is very sharp as is seen in Figs. 2 and 3.

For the $\Sigma^- p$ scattering cross sections, we have the reservation that the present calculation does not incorporate the Coulomb force. This is because the approximate treatment developed in pp and $\Sigma^+ p$ systems is not sufficient for incorporating the isospin symmetry breaking of the present coupled-channel system. One has to deal with the difference of the

threshold energies of the $\Sigma^- p$ and $\Sigma^0 n$ systems. Since the effect of the Coulomb force is less than $10 \sim 20$ % in the cross sections as is discussed in Ref. 12), we simply use the isospin relations to construct the scattering amplitudes with these particle bases. Figure 15 compares the calculated the total elastic cross sections for $\Sigma^- p$ scattering with the experimental data of Ref. 16). The calculation overestimates the experiment more than $40 \sim 50$ %, which is common to the quark-model study in Refs. 17), 15) and 18). Figure 16 shows the differential $\Sigma^- p$ elastic cross sections at $p_\Sigma = 160$ MeV/c. The calculation overestimates the magnitude, and does not fully reproduce the rather steep forward rise of the experimental data. The total reaction cross sections for the $\Sigma^- p \to \Sigma^0 n$ charge-exchange reactions are shown in Fig. 17, together with the experimental data of Ref. 19) and the unpublished data of the Massachusetts group[20]. The total reaction cross sections for $\Sigma^- p \to \Lambda n$ and the differential cross sections at $p_\Sigma = 160$ MeV/c are shown in Figs. 18 and 19, respectively, together with the data of Refs. 19) and 20). A reasonable agreement is obtained between theory and experiment, although more accurate determination of the cross sections is clearly indispensable for a detailed comparison.

§4. SUMMARY AND OUTLOOK

The final goal of this investigation is to achieve a unified description of the hyperon-nucleon (YN) interaction consistent with the nucleon-nucleon (NN) interaction by employing the compositeness of the octet baryons in terms of the quark degrees of freedom. Since hyperons and nucleons belong to the same class of the spin-flavor SU_6 supermultiplet 56, the rich flavor symmetry of the quark model is expected to provide a strong constraint on the internal consistency of the NN and YN interactions. In this and previous[3] papers, it is found that such a description is indeed possible, if the SU_6 quark model incorporates the full Fermi-Breit interaction with explicit flavor symmetry breaking, and is reinforced with the minimum effective meson-exchange potentials induced from the scalar-meson central attraction and π, K tensor force of the Nijmegen model-F potential. With two adjustable

parameters determined from the deuteron binding energy and $NN\ ^1S_0$ phase shift, all the low-energy cross sections of the hyperon-nucleon interaction currently available are reasonably reproduced in a unified RGM framework. We call this model RGM-F, since all the meson parameters are taken over from the Nijmegen model-F potential.

In this paper, we have discussed the system with the total hypercharge $Y = 1$ and the isospin $I = 1/2$; i.e., ΛN-$\Sigma N(I = 1/2)$ system, in which the channel-coupling effect of the ΛN and $\Sigma N(I = 1/2)$ configurations plays an important role. The effective meson-exchange potentials in the coupled-channel equation are constructed by following basically the same idea as adopted in the previous single-channel calculations in the NN and $\Sigma^+ p$ systems.[3] No further parameter fitting is made in the present coupled-channel calculation. By the careful elimination of the Pauli-forbidden component in the $^1S_0$ state, it is found that the ΛN-$\Sigma N(I = 1/2)$ channel-coupling effect is usually not significant except for some specific energy regions. One is the ΣN threshold region in the ΛN scattering, in which a cusp structure appears in the $^1S_0$ state. This cusp structure is strongly enhanced by the tensor force to show sharp step-like and dispersion-like resonance behavior in the $^3S_1$ and $^3D_1$ states, respectively. The effect of this threshold resonance on the Λp total cross sections is not strong, probably because the width is very small. On the other hand, the very strong antisymmetric $LS^{(-)}$ force characteristic in the quark-model study of the $I = 1/2$ system gives a prominant bump structure with a large width at the energy region slightly below the ΣN threshold. This is caused by the intriguing mechanism that the weak ^3P resonance in the $\Sigma N(I = 1/2)$ channel due to the effect of the Pauli principle is strongly enhanced in the $^3P_1$ channel by the $LS^{(-)}$ and the other non-central forces and that the developed resonance moves to the $^3P_1$ and $^1P_1$ states of the ΛN channel. The $^3P_1$ resonance is step-like and the $^1P_1$ resonance is dispersion-like in the present calculation.

In spite of the predictive feature of the present calculation, the qualitative aspect of the Λp resonance should not be overtrusted, since we have made a couple of simplifications to make this calculation possible. First of all, we have introduced rather weak flavor symmetry breaking by adopting $\lambda = m_s/m_{ud} = 1.25$. With this value of λ, the calculated threshold

energy of the ΣN channel in the ΛN scattering is only a half of the empirical value. Although the other half is expected to be accounted for by the effect of meson-exchange potentials, the present approximation is too crude to give the non-zero contribution to the internal energies of the constituent clusters. The choice of a larger λ value around $\lambda \sim 1.69$ does not seem to be permissible, if one tries to realize the intricate balance of the central attraction required in the overall reproduction of the ^1S phase-shift behavior of the NN, ΛN and ΣN systems. Furthermore, we have neglected the effect of the Coulomb force which is appreciable especially in the $\Sigma^- p$ system. In connection with this, we have to note that the $\Sigma^- p$ elastic cross section is already overestimated in the present calculation. It is possible that the central attraction of the $\Sigma N(I = 1/2)$ channel is too attractive in the present model. If the resonance in the $\Sigma^- p$ single-channel calculation is not so prominent as in the present case, it is very probable that the bump structure in the Λp total scattering cross section is much more suppressed than in the present calculation.

We have to stress, however, that the main purpose of the quark-model study is not actually the reproduction of the experimental data, but to study the many-body aspect of the quark-gluon dynamics manifested in the rich phenomena of the hadron-hadron interactions. Because of the restriction of the non-relativistic quark model, it is preferable to avoid the dynamical aspect of the quark confinement by assuming a simple harmonic-oscillator wave function for the spatial cluster functions and to concentrate on the symmetry aspects of the spin, flavor and color degrees of freedom. In this respect, the RGM framework is extremely convenient, since it can isolate contributions of particular pieces of the quark residual interaction through explicit evaluation of the quark-exchange diagrams. The most important finding of this investigation is that the short-range part of the NN and YN interactions is well described as the interaction between composite particles of quarks which interact to each other with the residual interaction exemplified by the color analog of the Fermi-Breit interaction. As for the relationship between the quark exchange effect and the vector-meson exchange effect, Ref. 21) should be referred to. By assuming that the phenomenological confinement potential is flavor independent, we have succeeded in reproducing the rich flavor

dependence of the hyperon-nucleon interaction in the short-range region with the standard values for the limited number of quark-model parameters. The dominant contribution comes from the color-magnetic and LS pieces of the Fermi-Breit interaction and the effect of the Pauli principle among quarks as well. After this details analysis of quark-model contributions, we can then proceed to studying the important meson-exchange effects in the medium- and long-range regions.

It is almost clear that we need more advanced treatment of the effective meson-exchange potentials. The replacement of the coupling constants at the baryon level, as well as the readjustment of the reduced mass to the empirical value, is not an entirely satisfactory procedure in the RGM framework. It is more desirable to reproduce the medium-range attraction and long-range tensor force through some appropriate quark-quark interactions. This is possibly achieved either by the evaluation of spin-flavor-color factors of the meson-exchange potentials between quarks or by the explicit introduction of the quark-antiquark excitations carried out in the study of the NN interaction [22),23)]. Although both of these directions need further analytical and numerical work, such an effort should be very fruitful since they will certainly lead to a new generation of the quark-model potentials for the YN interaction.

ACKNOWLEDGMENTS

The authors would like to thank members of Nuclear Theory Groups of Kyoto and Niigata Universities for useful discussions. They also would like to acknowledge the generous grants of computer time by the Research Center for Nuclear Physics, Osaka University. This work was supported by Grant-in-Aid for Scientific Research (C) from the Ministry of Education, Science and Culture (04640296).

REFERENCES

[1] See, for example, Nucl. Phys. **A547**, Nos. 1, 2 (1992) 243c ; *Proceedings of the U.S.-Japan Seminar on Properties and Interactions of Hyperons*, ed. B. F. Gibson, P. D. Barnes and K. Nakai (World Scientific, Singapore, 1994).

[2] C. Nakamoto, Y. Suzuki and Y. Fujiwara, submitted to Prog. Theor. Phys. (1995).

[3] Y. Fujiwara, C. Nakamoto and Y. Suzuki, submitted to Prog. Theor. Phys. (1995).

[4] Y. Fujiwara, C. Nakamoto and Y. Suzuki, in *Proceedings of the Second International Symposium on Medium Energy Physics*, ed. Weiqin Chao and Pengnian Shen (World Scientific, Singapore, 1995), p. 124.

[5] C. Nakamoto, Y. Suzuki and Y. Fujiwara, Phys. Letters **B318** (1993), 587.

[6] M. M. Nagels, T. A. Rijken and J. J. de Swart, Phys. Rev. **D20** (1979), 1633.

[7] M. Kamimura, Prog. Theor. Phys. Suppl. No. 62 (1977), 236.

[8] M. M. Nagels, T. A. Rijken and J. J. de Swart, Phys. Rev. **D15** (1977), 2547.

[9] Particle Data Group, Phys. Rev. **D50** (1994), Part 1.

[10] G. Alexander, U. Karshon, A. Shapira, G. Yekutieli, R. Engelmann, H. Filthuth and W. Lughofer, Phys. Rev. **173** (1968) 1452.

[11] B. Sechi-Zorn, B. Kehoe, J. Twitty and R. A. Burnstein, Phys. Rev. **175** (1968) 1735.

[12] A. Reuber, K. Holinde and J. Speth, Nucl. Phys. **A570** (1994) 543.

[13] See, for example, Section 9.4b. of K. Wildermuth and Y. C. Tang, *A Unified Theory of the Nucleus, Clustering Phenomena in Nuclei*, Vol. 1, ed. K. Wildermuth and P. Kramer (Vieweg, Braunschweig, Germany, 1977).

[14] J. A. Kadyk, G. Alexander, J. H. Chan, P. Gaposchkin and G. H. Trilling, Nucl. Phys. **B27** (1971), 13.

[15] Ulrich Straub, Zhang Zong-Ye, Kurt Bräuer, Amand Faessler, Surenda B. Khadkikar and Georg Lübeck, Nucl. Phys. **A508** (1990), 385c.

[16] F. Eisele, H. Filthuth, W. Föhlisch, V. Hepp and G. Zech, Phys. Letters **37B** (1971), 204.

[17] U. Straub, Zhang Zong-Ye, K. Bräuer, Amand Faessler, S. B. Khadkikar and G. Lübeck, Nucl. Phys. **A483** (1988), 686.

[18] Zong-ye Zhang, Amand Faessler, U. Straub and L. Ya. Glozman, Nucl. Phys. **A578** (1994), 573.

[19] R. Engelmann, H. Filthuth, V. Hepp and E. Kluge, Phys. Letters **21** (1966), 587.

[20] D. Stephen, Ph. D. thesis, Univ. of Massachusetts, 1970 (unpublished).

[21] K. Yazaki, Prog. Part. Nucl. Phys. **24** (1990), 353 ; *Perspectives of Meson Sciences*, eds. T. Yamazaki, K. Nakai and K. Nagamine (North-Holland, Amsterdam, 1992), p. 795.

[22] Y. Fujiwara and K. T. Hecht, Nucl. Phys. **A444** (1985), 541 ; **A451** (1986), 625 ; **A456** (1986), 669 ; **A462** (1987), 621 ; K. T. Hecht and Y. Fujiwara, Nucl. Phys. **A463** (1987), 255c.

[23] Y. Fujiwara, Prog. Theor. Phys. Suppl. No. 91 (1987), 160.

TABLES

TABLE I. The S-wave effective-range parameters for ΛN system derived from RGM-F and the other models; Nijmegen model-D [8], model-F [6], and Jülich models A and B [12]. Some results of the effective-range analysis are also shown in "exp't".

ΛN	a_s(fm)	r_s(fm)	a_t(fm)	r_t(fm)
RGM-F	−2.03	3.05	−1.66	3.26
model-D	−1.90	3.72	−1.96	3.24
model-F	−2.29	3.17	−1.88	3.36
model-A	−1.56	1.43	−1.59	3.16
model-B	−0.56	7.77	−1.91	2.43
exp't [10]	−1.8	2.8	−1.6	3.3
exp't [11]	−2.0	5.0	−2.2	3.5

Figure Captions

Fig. 1 : Calculated ΛN and $\Sigma N(I = 1/2)$ phase shifts for $^1S_0$ channel as a function of the incident momentum p_Λ in the laboratory system. The ΛN phase shift in the single-channel calculation is also shown in the dashed curve. The ΣN channel opens at the "theoretical" threshold energy of $p_\Lambda = 445.2$ MeV/c. The crosses denote Λp phase shift predicted by the Nijmegen model-F [6] in the full calculation.

Fig. 2 : Same as Fig. 1, but for $^3S_1$ channel. The $^3S_1$-$^3D_1$ coupling by the tensor force is included even in the ΛN single-channel calculation.

Fig. 3 : Same as Fig. 1, but for (a): ΛN phase shift in $^3D_1$ channel, and (b): the mixing parameter ϵ_1 for the ΛN $^3S_1$-$^3D_1$ coupling. The predictions by the Nijmegen model-D [8] are also shown by open circles.

Fig. 4 : The reflection and transmission coefficients η_{fi} for $J = 1$ even-parity states of ΛN-$\Sigma N(I = 1/2)$ system. The channels f and i are specified by 1: ΛN $^3S_1$, 2: ΛN $^3D_1$, 3: $\Sigma N(I = 1/2)$ $^3S_1$, and 4: $\Sigma N(I = 1/2)$ $^3D_1$. The coefficients in (a) are for ΛN $^3S_1$ incident channel and those in (b) are for $\Sigma N(I = 1/2)$ $^3S_1$ incident channel.

Fig. 5 : Calculated $\Sigma N(I = 1/2)$ phase shifts in $^3S_1$, $^3D_1$ and $^1S_0$ channels as a function of the incident momentum p_Σ in the laboratory system. The dashed curves denote the results of $\Sigma N(I = 1/2)$ single-channel calculations. The $^3S_1$ phase shift calculated with the ΣN central force only is also shown by the dotted curve.

Fig. 6 : Same as Fig. 4 (b), but as a function of the incident momentum p_Σ in the laboratory system. The result of the $\Sigma N(I = 1/2)$ single-channel calculation is also shown in the dashed curves.

Fig. 7 : Same as Fig. 1, but for $^1D_2$ and $^3D_2$ channels. The coupling by the $LS^{(-)}$ force is included.

Fig. 8 : Same as Fig. 1, but for $^3P_0$ channel.

Fig. 9 : Same as Fig. 1, but for $^3P_2$ channel. The Λp prediction by the Nijmegen model-D [8] is also shown by open circles.

Fig. 10 : Same as Fig. 1, but for $^1P_1$ channel. The coupling between $^1P_1$ and $^3P_1$ channels due to the $LS^{(-)}$ force is included even in the ΛN single-channel calculation.

Fig. 11 : Same as Fig. 1, but for $^3P_1$ channel. The coupling between $^1P_1$ and $^3P_1$ channels due to the $LS^{(-)}$ force is included even in the ΛN single-channel calculation.

Fig. 12 : The reflection (dashed curve) and transmission (solid curves) coefficients η_{fi} for $J = 1$ odd-parity states of ΛN-$\Sigma N(I = 1/2)$ system. The channels f and i are specified by 1: ΛN $^1P_1$, 2: ΛN $^3P_1$, 3: $\Sigma N(I = 1/2)$ $^1P_1$, and 4: $\Sigma N(I = 1/2)$ $^3P_1$. The incident channel is ΛN $^1P_1$.

Fig. 13 : $\Sigma N(I = 1/2)$ $^3P_1$ phase shifts in various approximations. Three types of single-channel $\Sigma N(I = 1/2)$ calculations are done by including the central force only (dotted curve), non-central forces except for the $LS^{(-)}$ force (dot-dashed curve), and the full non-central forces (dashed curve). The solid curve indicates the full calculation with both $^1P_1$-$^3P_1$ and $\Sigma N(I = 1/2)$-ΛN couplings included.

Fig. 14 : Calculated ΛN total elastic cross sections compared with the experimental data of Refs. 10), 11) and 14).

Fig. 15 : Calculated $\Sigma^- p$ total elastic nuclear cross sections compared with the experimental data of Ref. 16). The Coulomb force is not included.

Fig. 16 : Calculated $\Sigma^- p$ differential cross sections at $p_\Sigma = 160$ MeV/c compared with the experimental data of Ref. 16). The Coulomb force is not included.

Fig. 17 : Calculated $\Sigma^- p \to \Sigma^0 n$ total reaction cross sections compared with the experimental data of Refs. 19) and 20). The Coulomb force is not included.

Fig. 18 : Calculated $\Sigma^- p \to \Lambda n$ total reaction cross sections compared with the experimental data of Refs. 19) and 20). The Coulomb force is not included.

Fig. 19 : Calculated differential cross sections for $\Sigma^- p \to \Lambda n$ at $p_\Sigma = 160$ MeV/c compared with the experimental data of Ref. 19). The Coulomb force is not included.

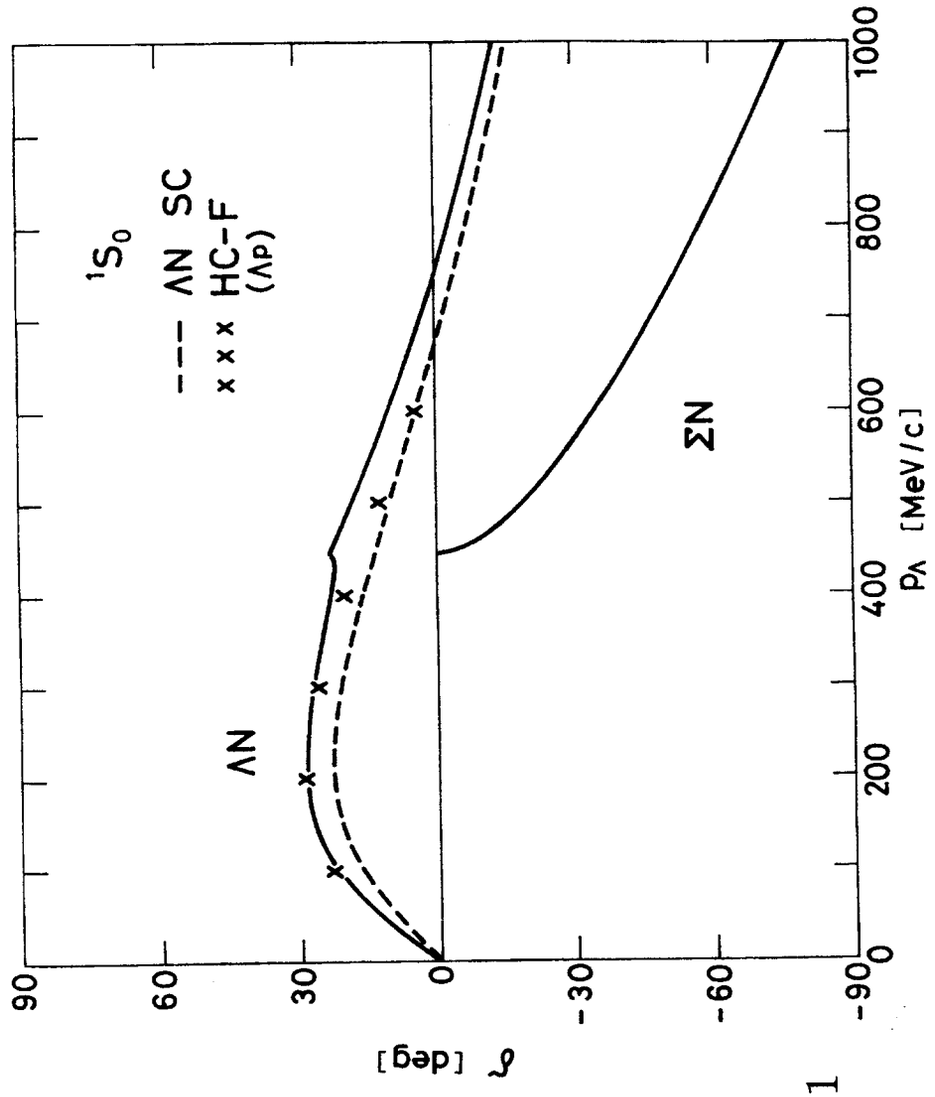

Fig. 1

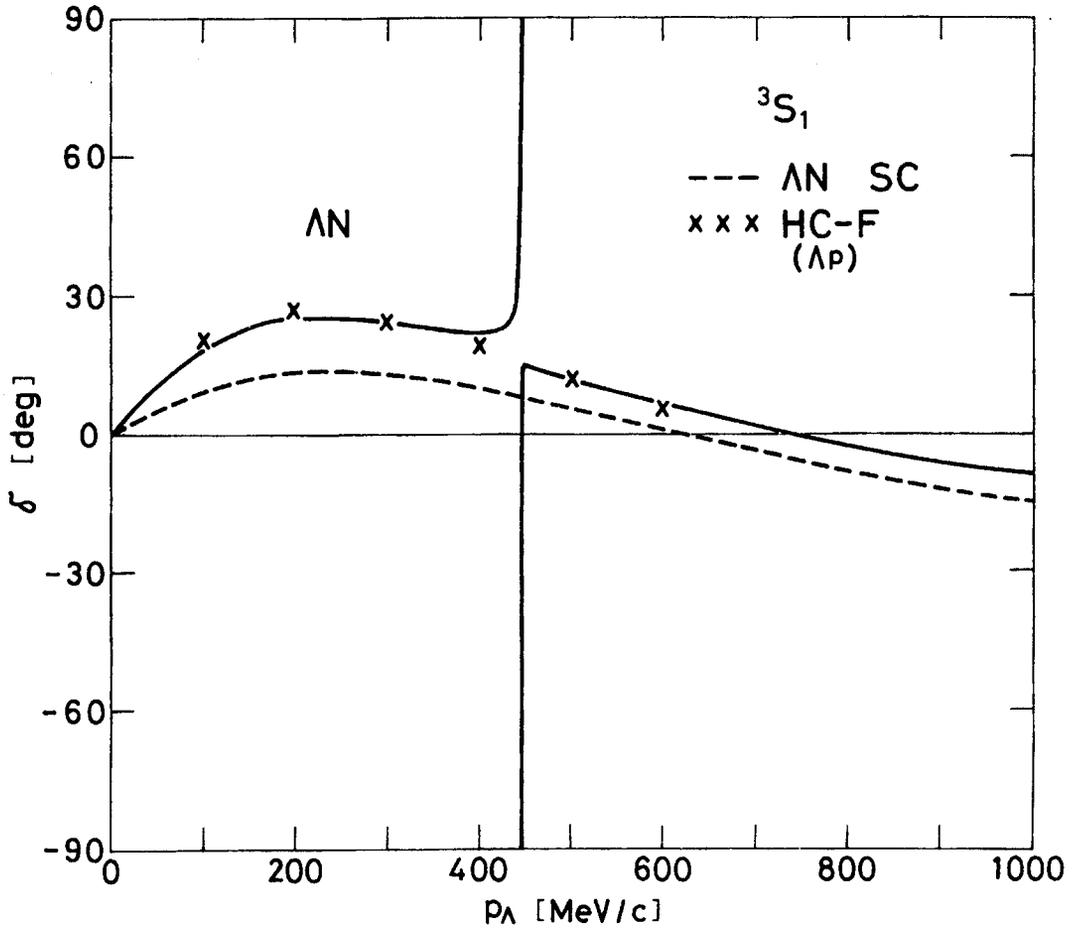
90
60
30
0
-30
-60
-90
δ [deg]
ΛN
$^3S_1$
--- ΛN SC
x x x HC-F
(ΛP)
0
200
400
600
800
1000
p_Λ [MeV/c]

Fig. 2

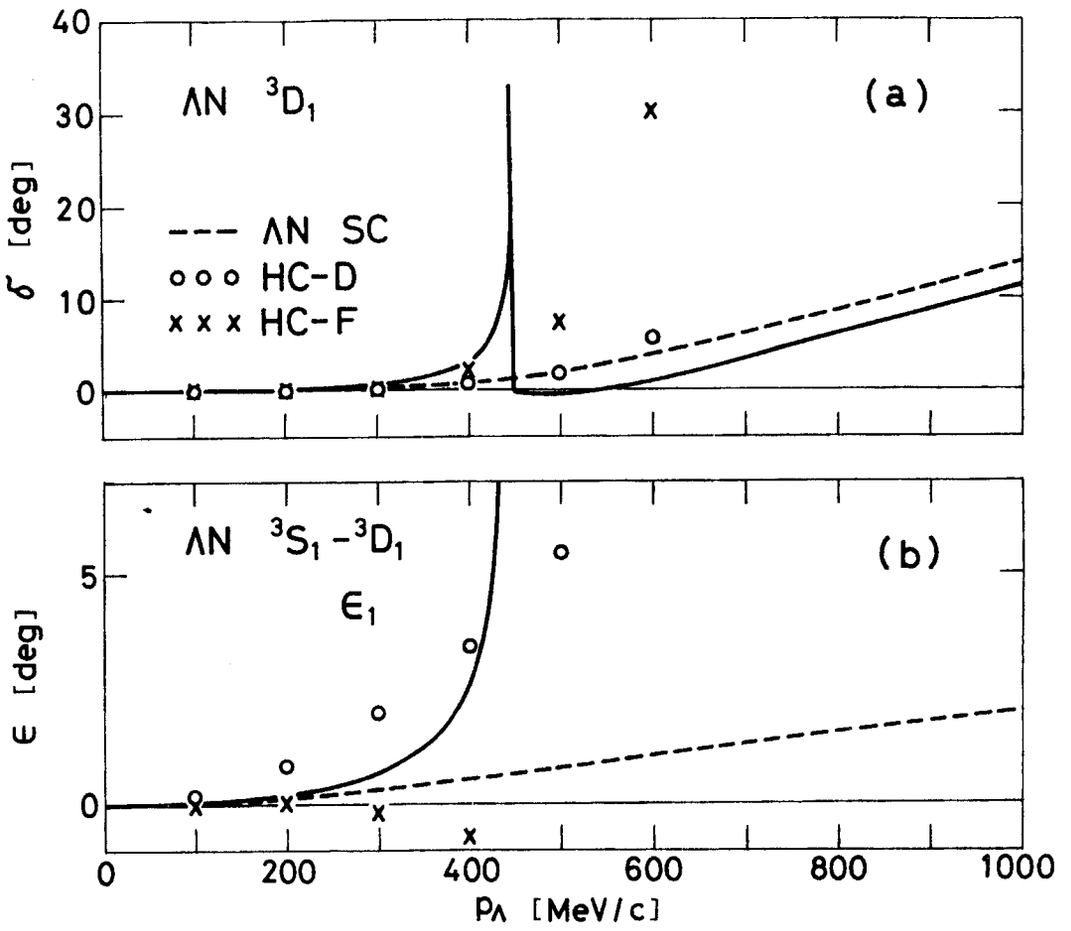
40
30
20
10
0
δ [deg]
ΛN $^3D_1$
(a)
--- ΛN SC
o o o HC-D
x x x HC-F
5
0
ε [deg]
ΛN $^3S_1 - ^3D_1$
ϵ_1
(b)
0
200
400
600
800
1000
p_Λ [MeV/c]

Fig. 3

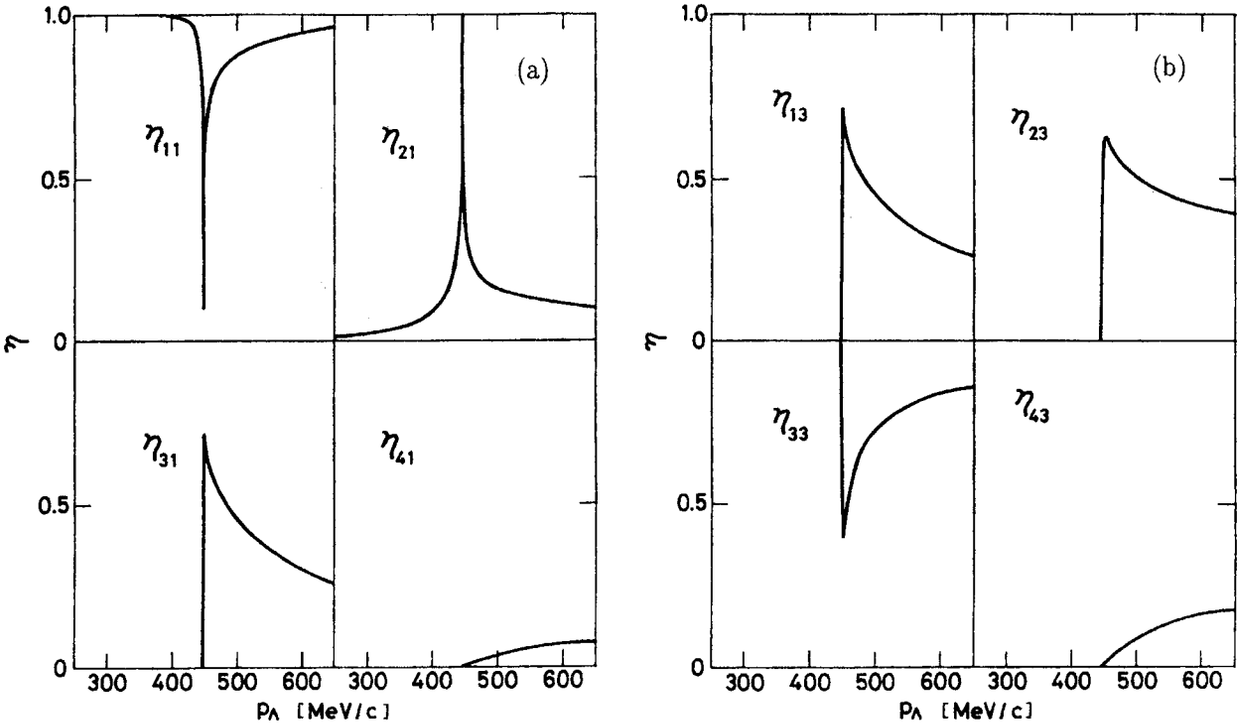
(a)
(b)
η_{11}
η_{21}
η_{31}
η_{41}
η_{13}
η_{23}
η_{33}
η_{43}
η
1.0
0.5
0
300 400 500 600
P_Λ [MeV/c]

Fig. 4

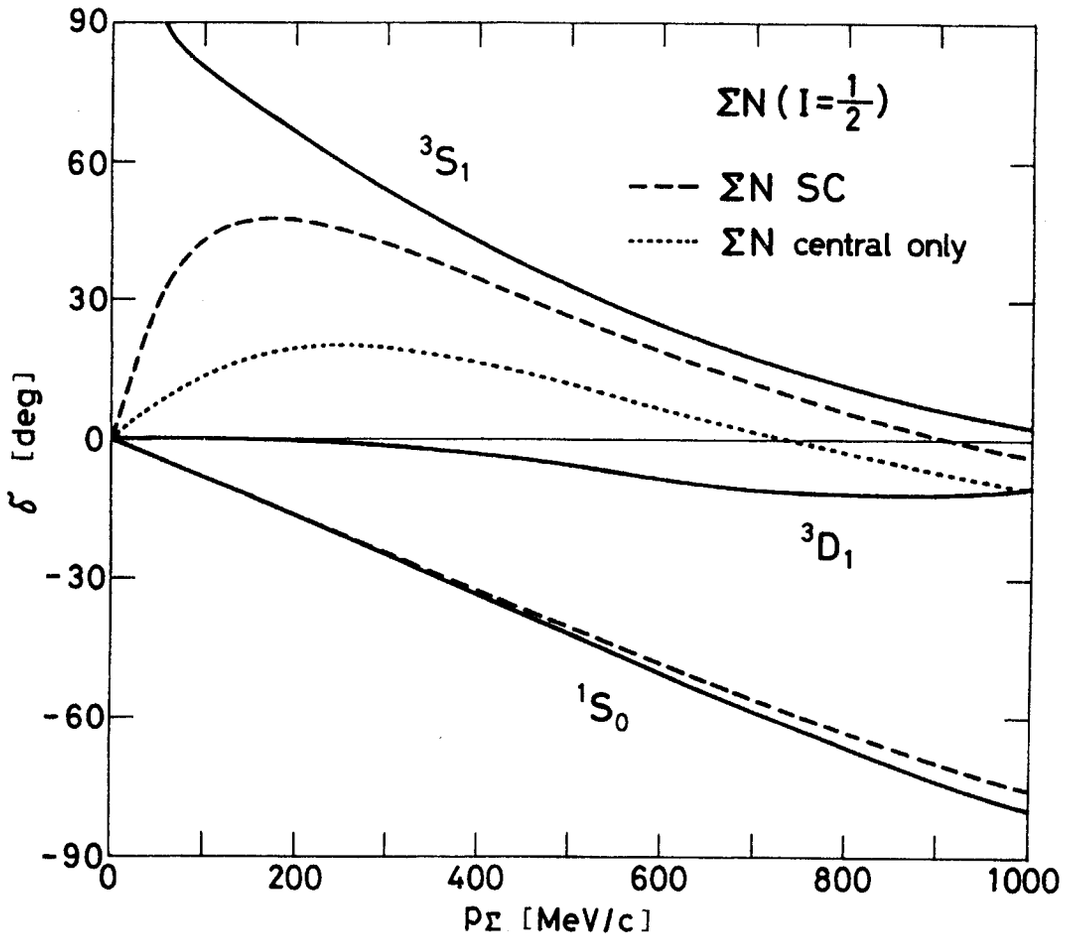
$\Sigma N\ (I=\frac{1}{2})$
$^3S_1$
$^3D_1$
$^1S_0$
--- ΣN SC
····· ΣN central only
δ [deg]
90
60
30
0
-30
-60
-90
0 200 400 600 800 1000
P_Σ [MeV/c]

Fig. 5

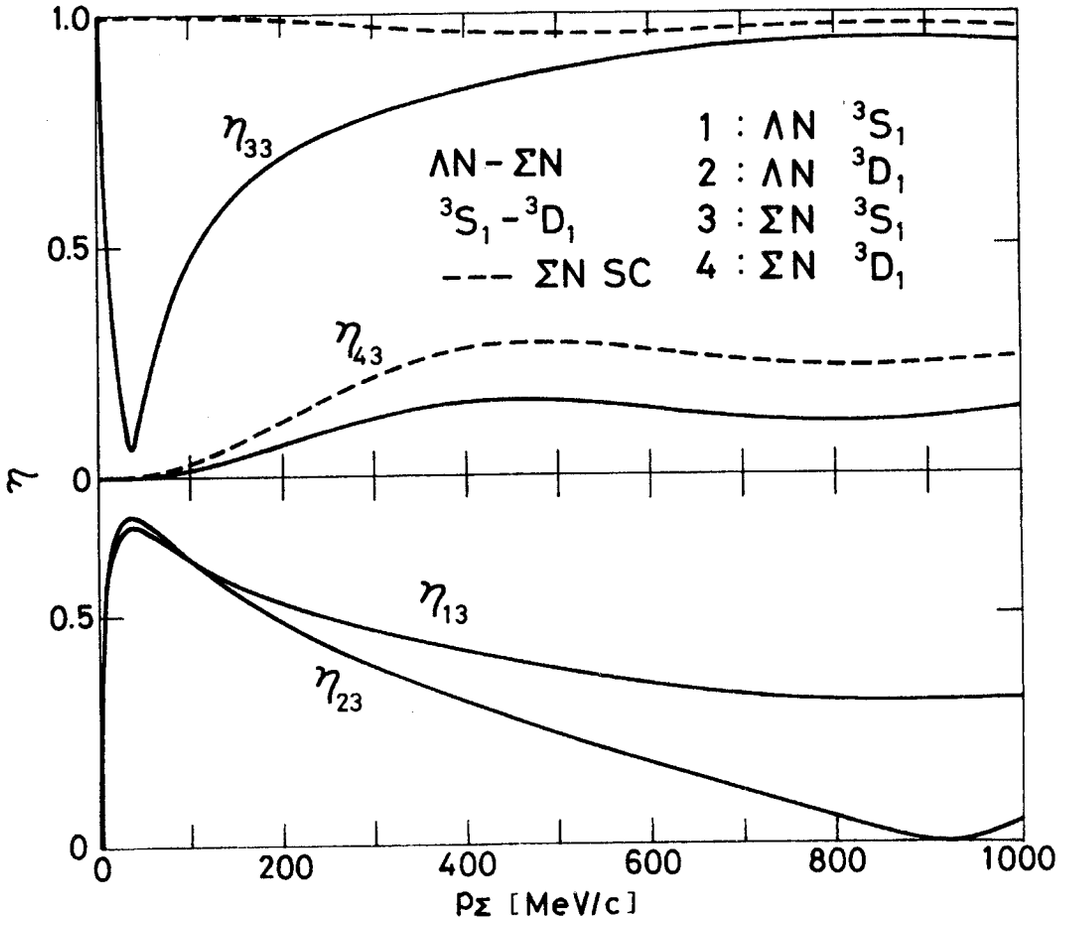
1.0
0.5
0
0.5
0
η
η33
η43
η13
η23
ΛN - ΣN
3S1 - 3D1
--- ΣN SC
1 : ΛN 3S1
2 : ΛN 3D1
3 : ΣN 3S1
4 : ΣN 3D1
0
200
400
600
800
1000
pΣ [MeV/c]

Fig. 6

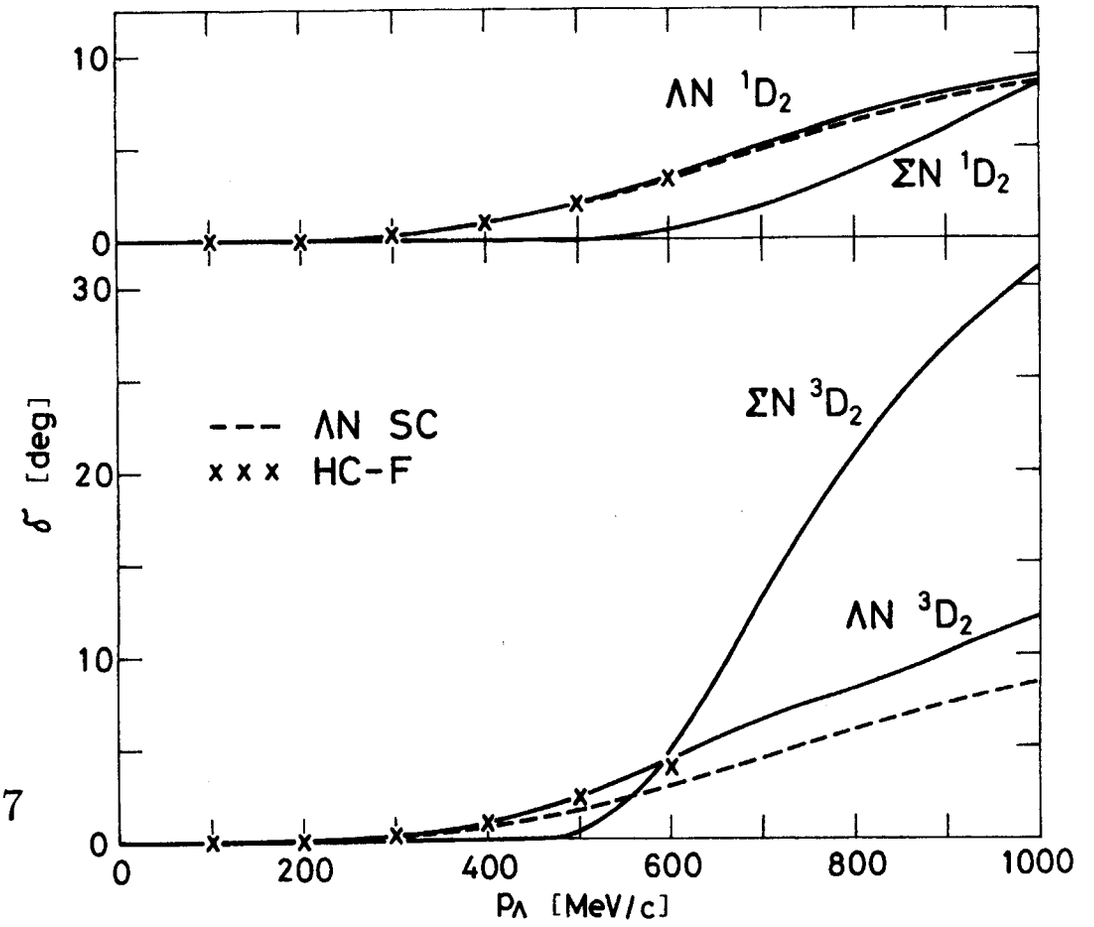
10
0
30
20
10
0
δ [deg]
ΛN 1D2
ΣN 1D2
ΣN 3D2
ΛN 3D2
--- ΛN SC
x x x HC-F
0
200
400
600
800
1000
pΛ [MeV/c]

Fig. 7

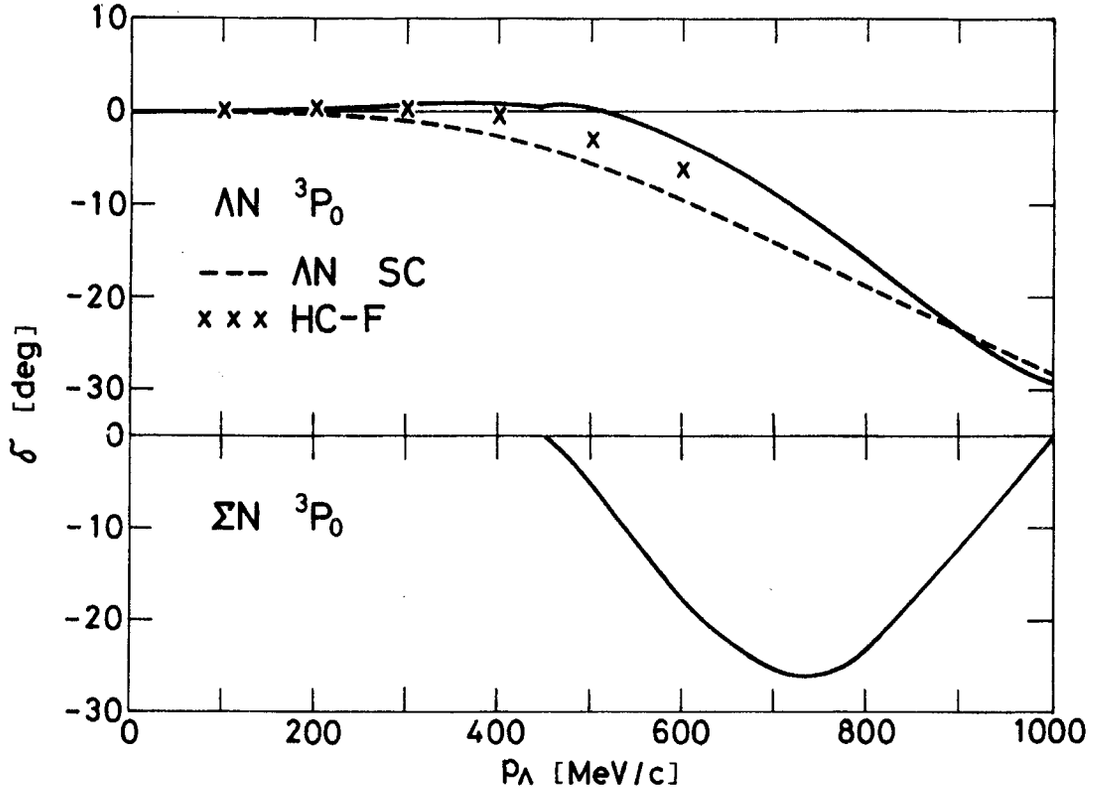
ΛN ³P₀
--- ΛN SC
x x x HC-F
ΣN ³P₀
δ [deg]
pΛ [MeV/c]

Fig. 8

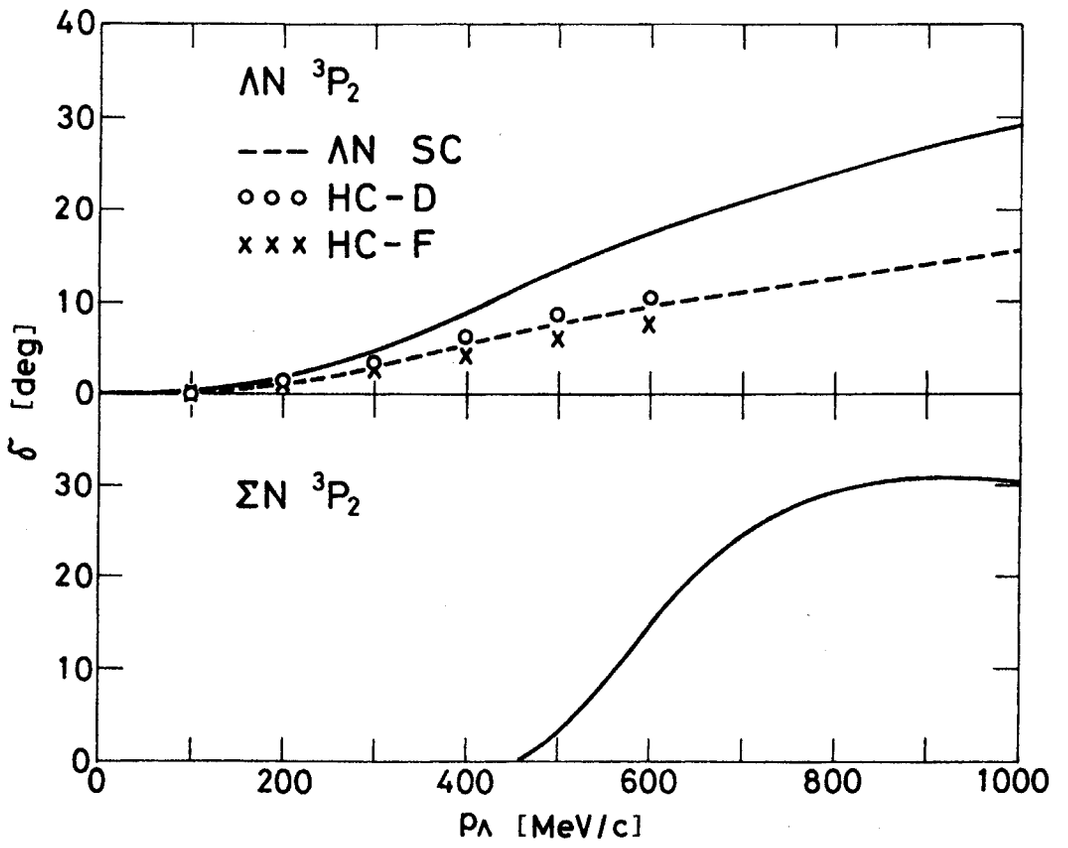
ΛN ³P₂
--- ΛN SC
o o o HC-D
x x x HC-F
ΣN ³P₂
δ [deg]
pΛ [MeV/c]

Fig. 9

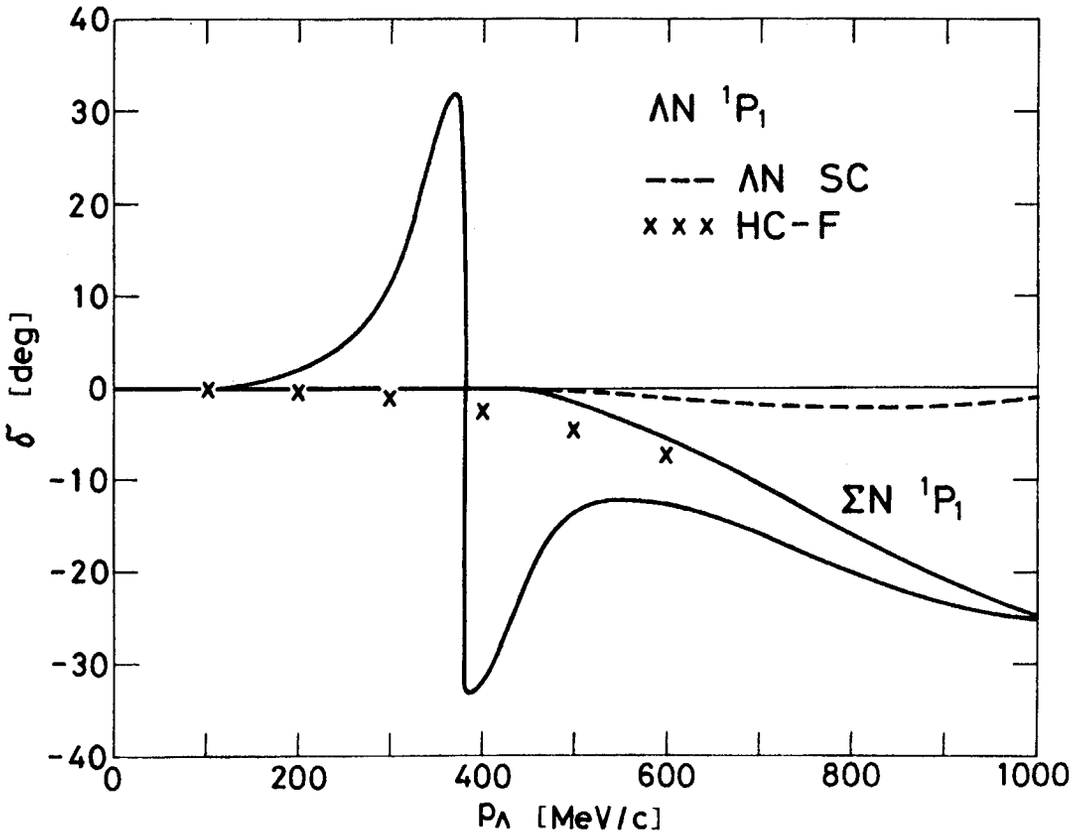
ΛN ¹P₁
--- ΛN SC
x x x HC-F
ΣN ¹P₁
δ [deg]
40
30
20
10
0
-10
-20
-30
-40
0
200
400
600
800
1000
Pᴧ [MeV/c]

Fig. 10

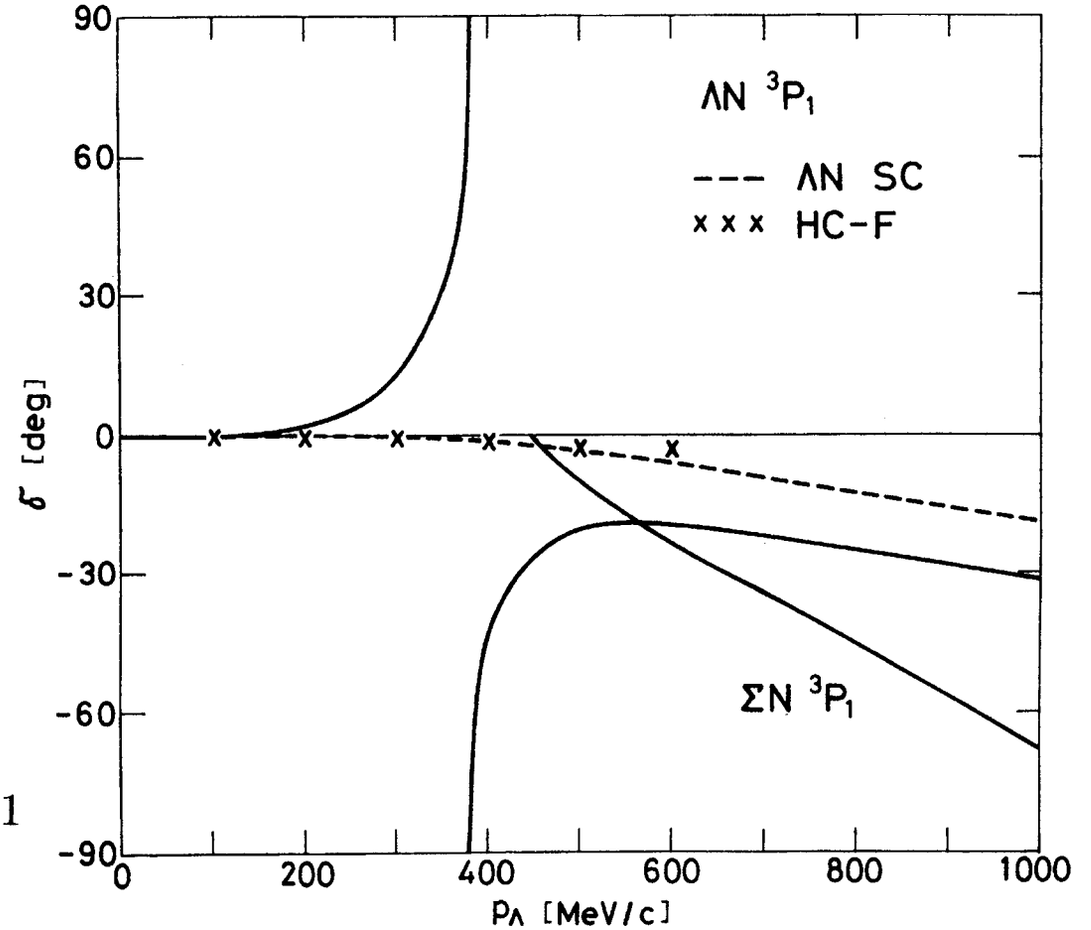
ΛN ³P₁
--- ΛN SC
x x x HC-F
ΣN ³P₁
δ [deg]
90
60
30
0
-30
-60
-90
0
200
400
600
800
1000
Pᴧ [MeV/c]

Fig. 11

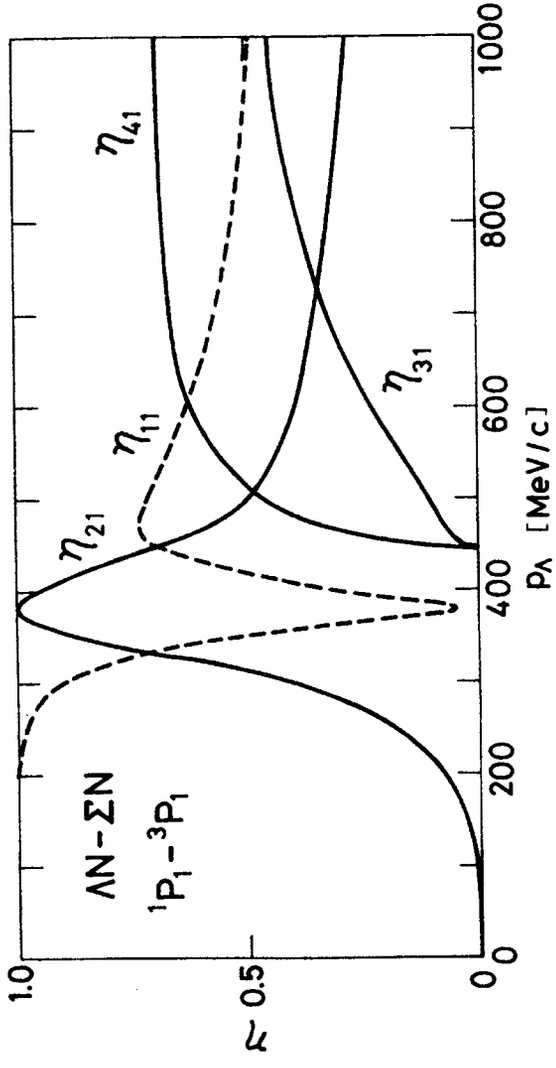
ΛN-ΣN
$^1P_1$-$^3P_1$
η_{41}
η_{11}
η_{21}
η_{31}
1.0
0.5
0
μ
0
200
400
600
800
1000
p_Λ [MeV/c]

Fig. 12

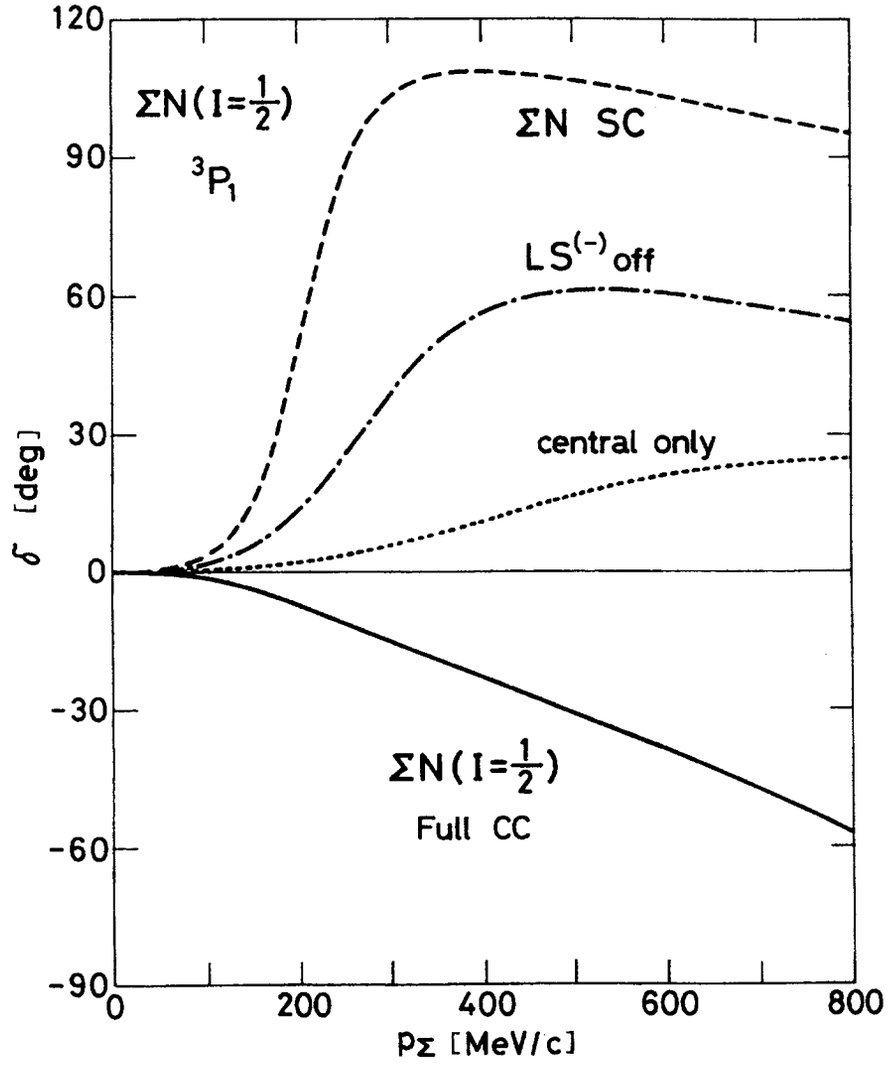
ΣN(I=1/2)
$^3P_1$
ΣN SC
LS$^{(-)}$off
central only
ΣN(I=1/2)
Full CC
δ [deg]
120
90
60
30
0
-30
-60
-90
0
200
400
600
800
p_Σ [MeV/c]

Fig. 13

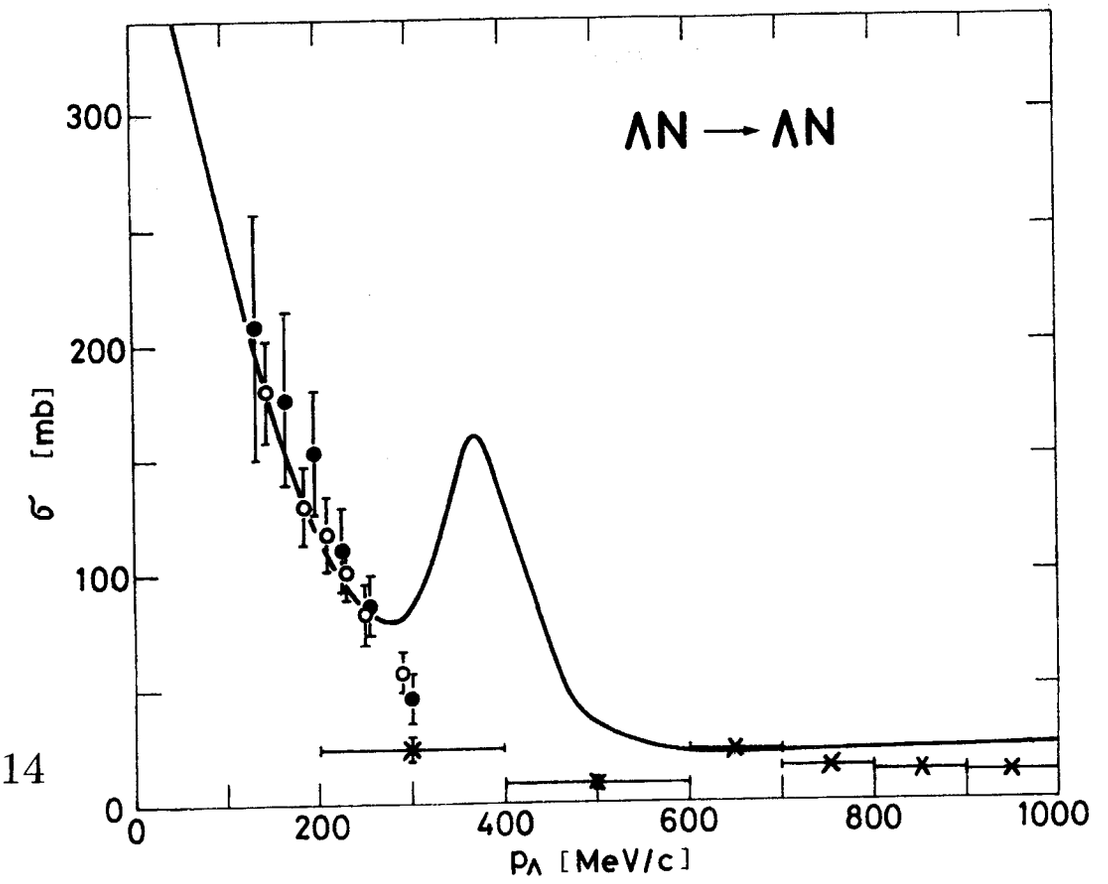
ΛN → ΛN
σ [mb]
300
200
100
0
0
200
400
600
800
1000
pΛ [MeV/c]

Fig. 14

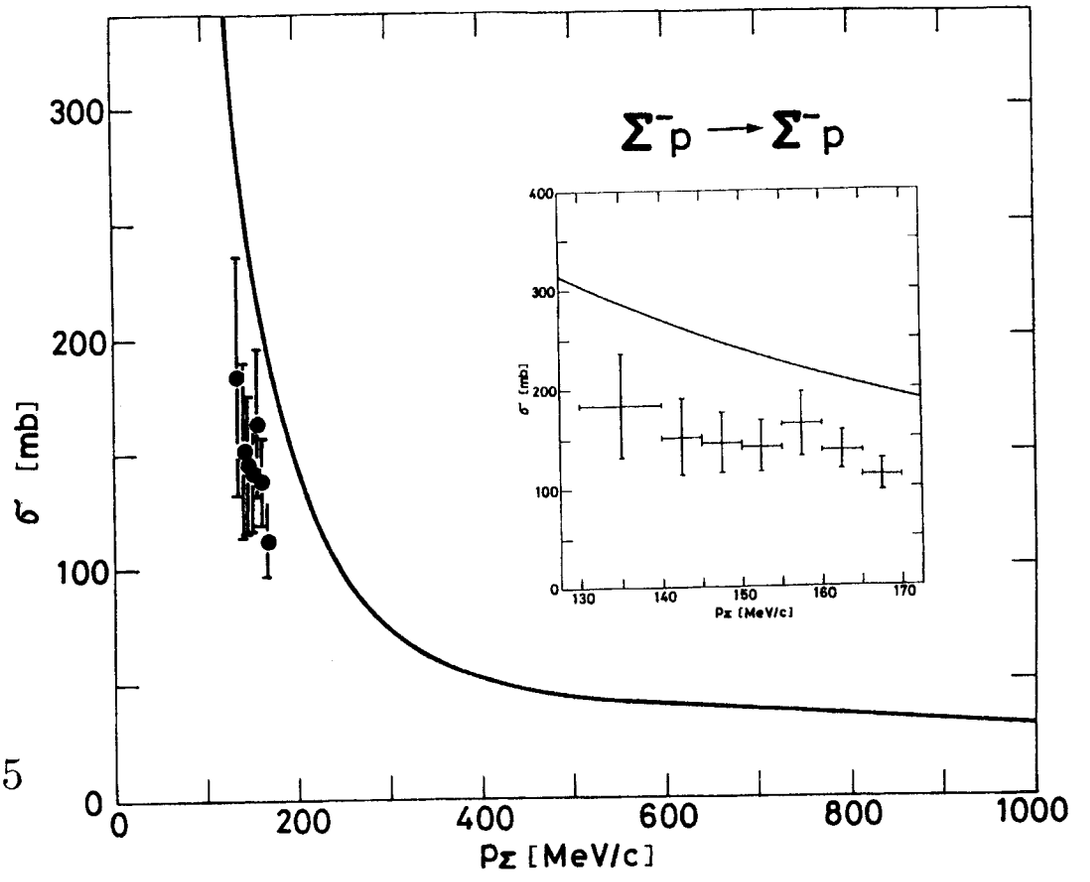
Σ⁻p → Σ⁻p
σ [mb]
300
200
100
0
0
200
400
600
800
1000
pΣ [MeV/c]
400
300
200
100
0
130
140
150
160
170
pΣ [MeV/c]

Fig. 15

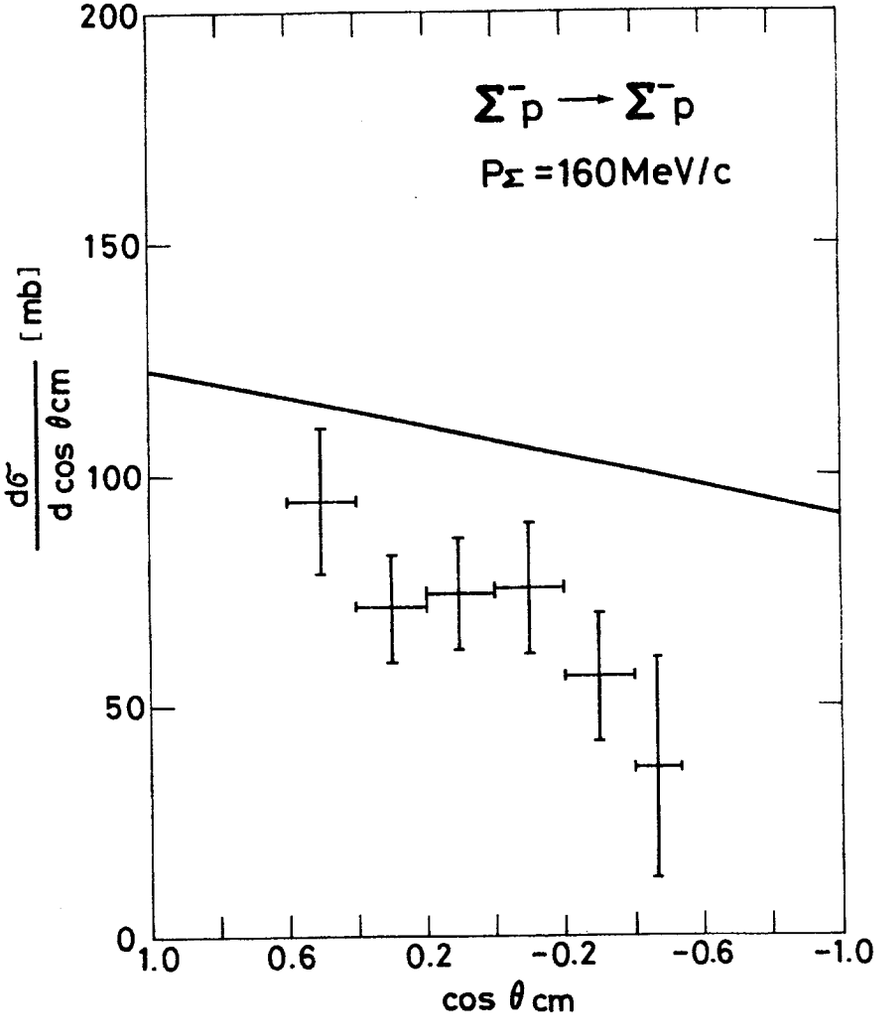
$\Sigma^- p \rightarrow \Sigma^- p$
P_Σ =160MeV/c
$\frac{d\sigma}{d\cos\theta cm}$ [mb]
200
150
100
50
0
1.0
0.6
0.2
-0.2
-0.6
-1.0
cos θ cm

Fig. 16

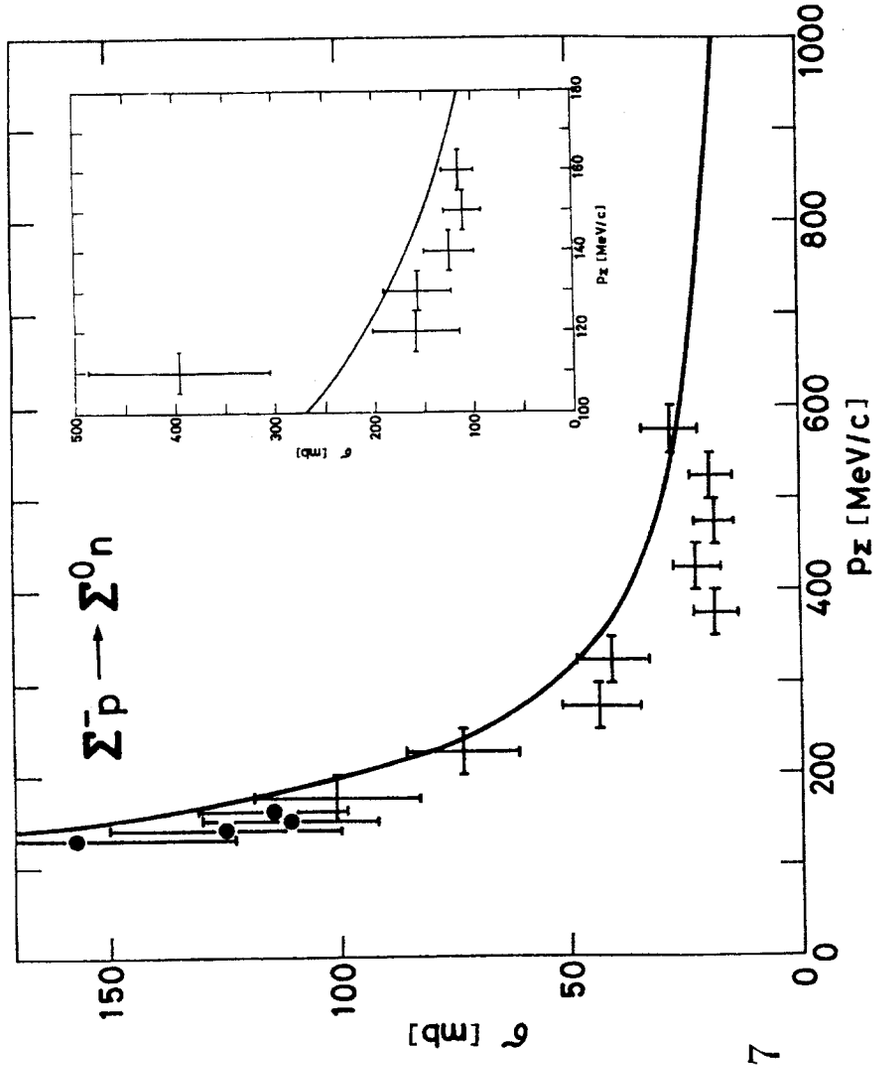
$\Sigma^- p \rightarrow \Sigma^0 n$
σ [mb]
150
100
50
0
Pz [MeV/c]
1000
800
600
400
200
0
500
400
300
200
100
0
180
160
140
120
100
Pz [MeV/c]

Fig. 17

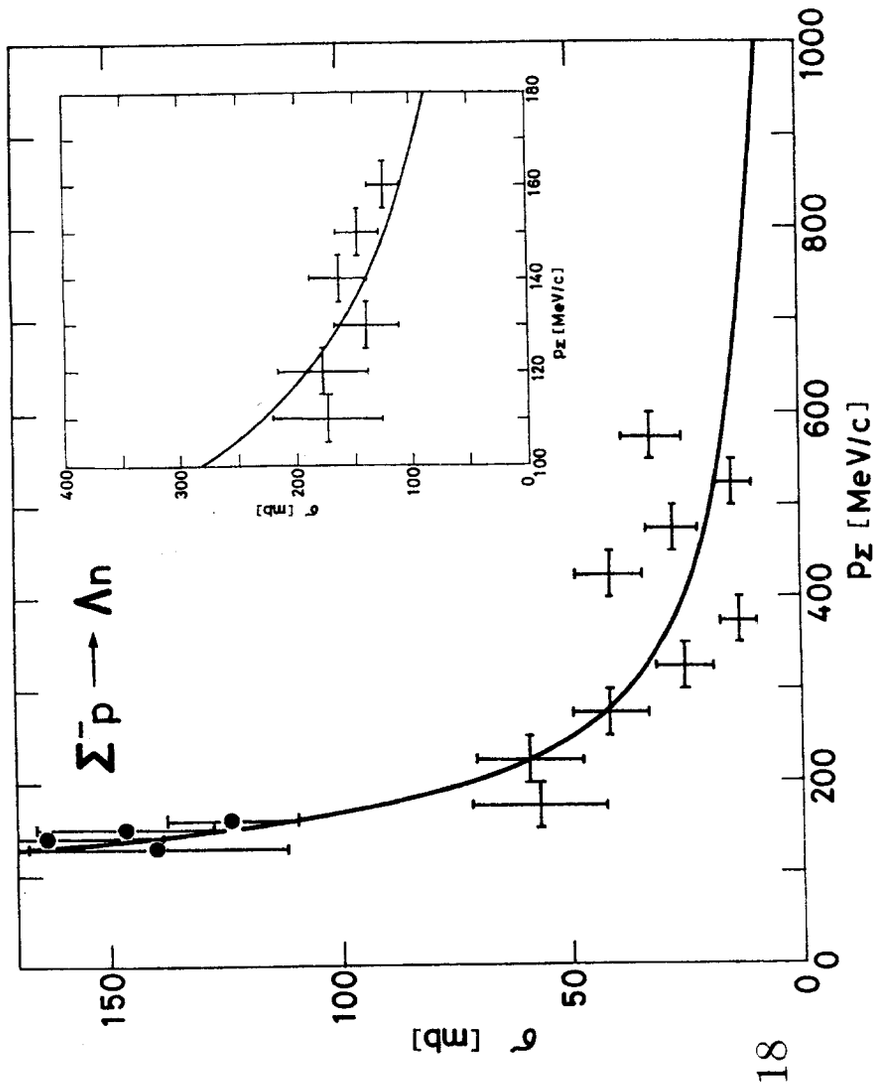
Σ⁻p → Λn
σ [mb]
Pσ [MeV/c]
0
50
100
150
200
400
600
800
1000
100
120
140
160
180
200
300
400

Fig. 18

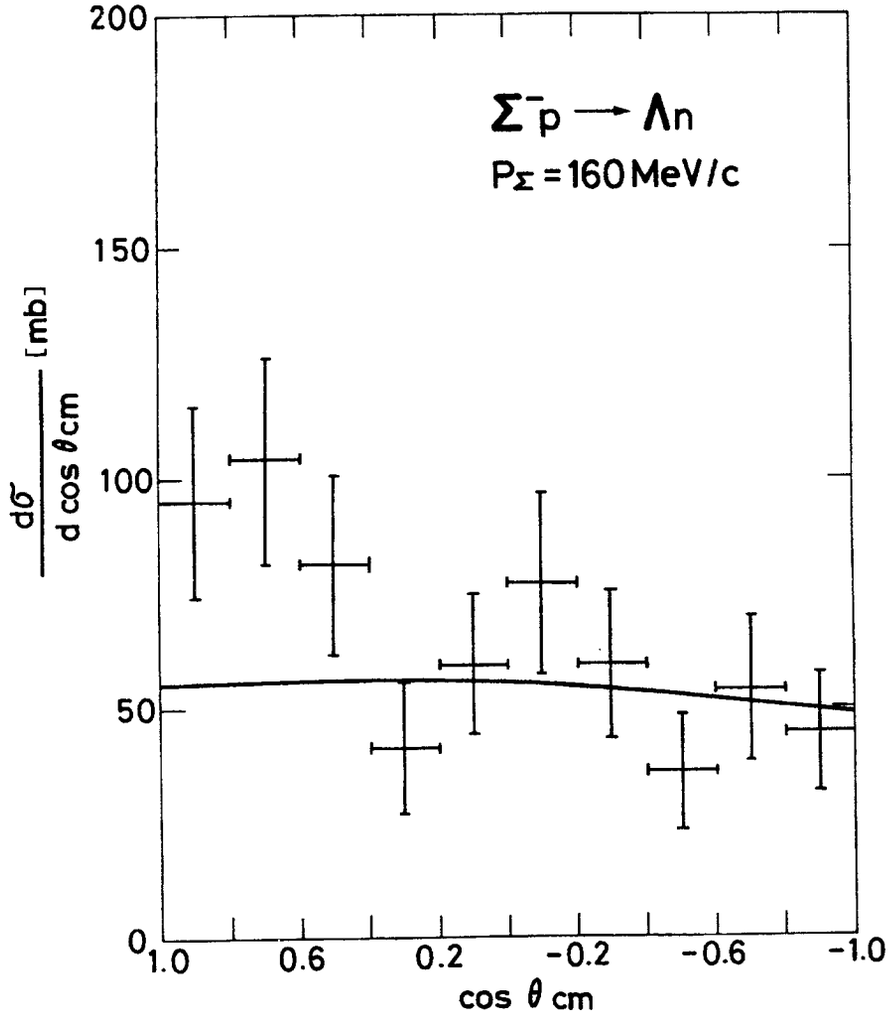
Σ⁻p → Λn
PΣ = 160 MeV/c
dσ/d cos θcm [mb]
cos θ cm
0
50
100
150
200
1.0
0.6
0.2
-0.2
-0.6
-1.0

Fig. 19